

A Doeblin-Anchored Contrastive Chart for Learning Markov Transition Kernels

Ao Xu*

XUAO24@MAILS.JLU.EDU.CN

School of Artificial Intelligence

Jilin University

No. 2699, Qianjin Street, Chaoyang District

Changchun 130012, China

and

Zhongguancun Academy

Daniufang 2nd Ring Road, Haidian District

Beijing 100094, China

Abstract

Learning a Markov transition model is not merely conditional density estimation: the learned object must be a valid transition kernel before it is iterated in downstream dynamics. This paper introduces a Doeblin-anchored contrastive chart, a statistical-to-dynamical coordinate framework for learning transition kernels from contrastive objectives. Given a restart law and an anchor strength, the chart mixes the target transition with the restart law. The resulting anchored kernel is simultaneously a Doeblin-minorized Markov kernel, the positive conditional law in a binary contrastive experiment, and an explicitly invertible coordinate for the original transition law. We prove that the anchored contrastive risk identifies the anchored transition density and calibrates excess risk to density error. Since inversion of a learned score may produce a signed or unnormalized object, we introduce a measurable Markovization operator that restores kernel validity while preserving integrated L^1 accuracy up to a constant factor. Oracle inequalities and Hölder-ReLU approximation bounds yield nonparametric rates for independent transition pairs. For stationary geometrically β -mixing trajectories, a conservative thinning-and-coupling extension yields the same reconstruction interface with an effective sample size. Occupancy-weighted perturbation bounds transfer one-step kernel error to finite-horizon marginal, path-law, and occupation-measure errors under explicit coverage.

Keywords: contrastive learning, Markov kernel, Doeblin minorization, noise-contrastive estimation, nonparametric transition density estimation

1 Introduction

Markov transition models are used not only for one-step prediction, but also for simulation, multistep forecasting, occupation measures, and stationary summaries. This makes transition learning different from ordinary conditional density estimation. A statistical procedure may fit a conditional density under a convenient loss, while leaving unclear whether the learned object is a valid transition kernel or which transition-kernel metric is controlled. Conversely, classical perturbation theory for Markov chains usually starts from two valid kernels and studies how a given kernel error propagates to marginals, path laws, or invariant

*. Corresponding author.

distributions (Meyn and Tweedie, 2009; Mitrophanov, 2005). The problem considered here lies at the interface of these two viewpoints: how can a transition law be learned through a contrastive statistical objective while still producing a valid Markov kernel whose error has dynamical meaning?

Contrastive density estimation provides a natural statistical route. Noise-contrastive estimation reduces density learning to binary classification against a known reference law (Gutmann and Hyvärinen, 2012), and conditional variants extend this idea to conditional and unnormalized models (Ceylan and Gutmann, 2018). More broadly, density-ratio estimation views such objectives as ways to learn ratios relative to a reference distribution (Sugiyama et al., 2012). Recent anchored contrastive constructions for ordinary density estimation show that mixing a target density with a reference density can create an interior object with a calibration inequality and an explicit de-anchoring map (Li and Lin, 2026). For Markov transition densities, however, the conditioning variable and the downstream use of the learned object introduce additional structure. It is not enough to contrast each conditional density separately. One must specify which conditional law is learned, how it reconstructs the original transition kernel, whether the reconstruction is itself a valid kernel, and how the resulting error propagates through the Markov dynamics.

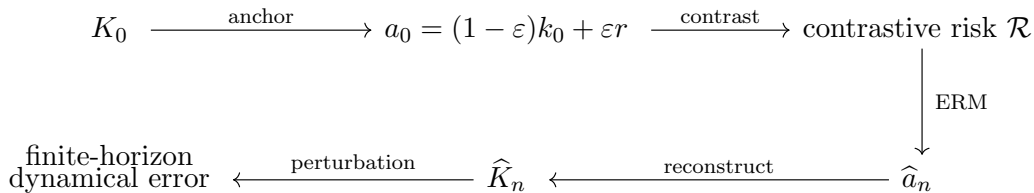
This paper introduces a Doeblin-anchored contrastive chart for transition-kernel learning. Given a restart law ν and an anchor strength ε , the chart maps a transition kernel K to the anchored kernel

$$A_{\varepsilon,\nu}K = (1 - \varepsilon)K + \varepsilon\nu.$$

The point of this construction is not merely to regularize the transition density. The anchored object has three simultaneous interpretations. First, it is a genuine Markov kernel satisfying a Doeblin minorization, a classical condition in Markov chain theory (Meyn and Tweedie, 2009; Nummelin, 1978). Second, it is the positive conditional law in a binary contrastive experiment against the restart reference. Third, it is an explicitly invertible coordinate for the original transition law, with inverse $(A - \varepsilon\nu)/(1 - \varepsilon)$. Thus the restart anchor provides a common coordinate system in which contrastive estimation, kernel reconstruction, and Markov perturbation analysis act on the same object.

This viewpoint turns contrastive transition learning into a validity-preserving reconstruction problem. A learned contrastive score estimates the anchored density, not directly the original transition density. Applying the inverse chart then produces a de-anchored transition score, but this score need not be nonnegative or row-normalized. This difficulty is largely absent from standard conditional density estimation, where the target is usually a one-step density or score (Hall et al., 1999; Hyndman and Yao, 2002; Chen, 2007), but it is essential for Markov dynamics, where the learned object must be iterated. We therefore introduce a deterministic Markovization map that clips and renormalizes each row. The map restores transition-kernel validity while preserving integrated L^1 accuracy up to a constant factor. The resulting estimator is therefore not only a contrastive score: it is a valid Markov kernel to which finite-horizon perturbation bounds can be applied.

The main idea is summarized by the following diagram.



The diagram should be read as a coordinate framework rather than as a single estimator. The upper row defines the population chart, while the lower row describes the reconstruction path followed by the estimator. The analysis proves quantitative stability along the arrows: contrastive excess risk controls anchored-density error, de-anchoring and Markovization convert this into valid-kernel error, and occupancy-weighted perturbation transfers valid-kernel error to finite-horizon dynamical error.

Beyond the basic reconstruction theorem, the framework admits standard statistical and dynamical extensions without changing the interface. Hölder–ReLU approximation and entropy bounds yield nonparametric transition-density rates, while a conservative thinning-and-coupling argument extends the oracle-to-reconstruction interface to stationary geometrically β -mixing trajectories through an effective sample size. A rare-state example clarifies why finite-horizon coverage assumptions cannot be dropped.

The contributions of the paper can be summarized as follows.

- **A contrastive Doeblin chart for transition kernels.** We introduce an exact coordinate dictionary between original transition kernels, Doeblin-minorized anchored kernels, contrastive posterior coordinates, and de-anchored reconstruction coordinates. The same restart law therefore serves simultaneously as a Markov-chain minorization device, a contrastive reference law, and a reconstruction coordinate.
- **Risk geometry and statistical learning in the chart.** We prove that the anchored contrastive risk has the anchored transition density as its unique population minimizer, admits an integrated Bernoulli–KL representation, and calibrates excess contrastive risk to anchored and de-anchored density error. Standard oracle inequalities and Hölder–ReLU approximation bounds can then be inserted into this geometry to obtain nonparametric transition-density rates. A conservative thinning-and-coupling argument also extends the same oracle-to-reconstruction interface to a thinned ERM based on stationary geometrically β -mixing trajectories, replacing the nominal sample size by an effective sample size.
- **Validity-preserving reconstruction.** We show that applying the inverse chart to a learned score may leave the cone of Markov kernels, producing a signed or unnormalized object. To close this gap, we introduce a measurable Markovization operator that restores nonnegativity and row normalization while preserving integrated L^1 accuracy up to a constant factor.
- **Dynamical transfer and diagnostic validation.** We connect the reconstructed kernel to downstream Markov dynamics by combining the one-step reconstruction error with occupancy-weighted perturbation bounds. This yields finite-horizon marginal,

path-law, and occupation-measure guarantees under explicit coverage. The experiments are designed as diagnostics for the full statistical-to-dynamical interface, including calibration, validity repair, anchor-strength tradeoffs, trajectory stress tests, and coverage-failure examples.

2 Related Work

This section positions the paper relative to six lines of work: contrastive density estimation, conditional and transition density estimation, Doeblin minorization and Markov perturbation theory, learning stochastic dynamics, oracle inequalities, and neural sieve rates.

Noise-contrastive and conditional contrastive density estimation. Noise-contrastive estimation reduces density estimation to binary classification against a known reference law (Gutmann and Hyvärinen, 2012), with conditional variants allowing the noise distribution to depend on the covariate (Ceylan and Gutmann, 2018). Density-ratio estimation gives a broader perspective on such objectives (Sugiyama et al., 2012). Recent data-augmented contrastive methods anchor an ordinary density to a reference density before applying a contrastive risk, yielding calibration and an explicit de-anchoring map (Li and Lin, 2026). The present paper uses the reference law in a transition setting where it is simultaneously the contrastive reference and the restart law in the Doeblin anchor $A_{\varepsilon,\nu}K = (1 - \varepsilon)K + \varepsilon\nu$.

Transition density and conditional density estimation. Nonparametric conditional density estimation includes kernel and local methods (Hall et al., 1999; Hyndman and Yao, 2002; Hall et al., 2004), single-index and other structural approaches (Hall and Yao, 2005), and general sieve estimators (Chen and Shen, 1998; Chen, 2007). Transition-density estimation for Markov processes has also been studied in econometrics and time series, including diffusion likelihood expansions (Aït-Sahalia, 2002) and spectral methods for stationary Markov processes (Hansen et al., 1998). Minimax theory for conditional density estimation identifies the role of smoothness in both variables (Li et al., 2022), while neural conditional density models include mixture density networks, conditional flows, and basis-expansion estimators (Bishop, 1994; Trippe and Turner, 2018; Izbicki and B. Lee, 2017; Gao and Hastie, 2022). These works primarily target one-step density accuracy; the additional issue here is that the learned object must be reconstructed as a valid transition kernel before it is iterated.

Doeblin minorization and Markov perturbation theory. Doeblin minorization is a classical device in Markov chain theory (Meyn and Tweedie, 2009). Restart and regeneration constructions, including Nummelin splitting, use related affine mixtures to analyze Harris recurrent chains (Nummelin, 1978). The Dobrushin coefficient describes contraction and forgetting of initial conditions (Dobrushin, 1956), while sensitivity of invariant laws under kernel perturbations has been developed for uniformly ergodic and operator-theoretic regimes (Mitrophanov, 2005; Kartashov, 1996). In this paper the same affine restart map is used as a statistical coordinate: the anchored kernel is the positive class in the contrastive experiment, and de-anchoring is the explicit inverse coordinate map.

Learning stochastic dynamics. Model-based reinforcement learning and probabilistic forecasting learn stochastic transition models for rollout, planning, or simulation (Ha and

Schmidhuber, 2018; Hafner et al., 2020; Chua et al., 2018). Rollout degradation under learned models is well known empirically (Talvitie, 2014), and one-step-to-multistep error bounds appear in model-based policy optimization (Janner et al., 2019). The present work is not a new dynamics algorithm or benchmark; it studies how a contrastive statistical objective can produce a valid kernel to which finite-horizon perturbation bounds apply under explicit coverage.

Oracle inequalities and fast rates. Empirical risk minimization with localized complexity measures, Rademacher bounds, Bernstein conditions, and validation-based selection is a standard route to oracle inequalities and fast rates (Bartlett and Mendelson, 2002; Bartlett et al., 2005; Tsybakov, 2004; Koltchinskii, 2006; Lecué and Mitchell, 2012). For dependent observations, blocking and coupling under absolute regularity provide a classical route from trajectory samples to effective independent sample sizes; see Doukhan (1994). These tools supply the statistical front end of the paper once the anchored contrastive risk has been placed in a bounded calibrated chart.

Neural sieve rates and minimax lower bounds. Deep ReLU networks achieve near-minimax rates for Hölder function classes under standard approximation and compositional assumptions (Yarotsky, 2017; Schmidt-Hieber, 2020). Covering-number bounds for neural network classes connect these approximations to estimation error (Anthony and Bartlett, 1999; Bartlett et al., 2019), while classical minimax theory supplies matching lower-bound constructions (Stone, 1982). The Hölder–ReLU part of the paper instantiates these ideas for bounded transition densities and then transports the resulting rate through de-anchoring and Markovization.

Summary of positioning. The individual components above are classical or already well developed in isolation: contrastive estimation, Doeblin minorization, empirical-process oracle inequalities, Markov perturbation bounds, and neural sieve rates. The contribution here is the interface that makes them act on the same transition-learning object. The restart anchor creates a chart between original kernels, Doeblin-minorized kernels, and contrastive posterior coordinates; risk calibration controls the anchored density; de-anchoring and Markovization produce a valid kernel for the original transition law; and occupancy-weighted perturbation transfers one-step kernel error to finite-horizon dynamical error under explicit coverage. The trajectory extension and rare-state example clarify the sampling and coverage boundaries of this interface.

3 Setup

3.1 Dominated transition kernels

Let $(\mathsf{X}, \mathcal{X})$ be a standard Borel measurable space. Throughout the statistical results we additionally assume that λ is a probability measure on $(\mathsf{X}, \mathcal{X})$ and that all transition kernels considered below are dominated by λ . A Markov kernel K from X to X is a map $K : \mathsf{X} \times \mathcal{X} \rightarrow [0, 1]$ such that $K(x, \cdot)$ is a probability measure for every x and $x \mapsto K(x, B)$ is measurable for every $B \in \mathcal{X}$. We write

$$K(x, dy) = k(y | x)\lambda(dy)$$

when $k : \mathsf{X} \times \mathsf{X} \rightarrow [0, \infty)$ is jointly measurable and $\int k(y | x) \lambda(dy) = 1$ for every x . Once a present-state design law μ is fixed below, equalities between densities are understood $\mu \otimes \lambda$ -almost everywhere unless a pointwise representative is explicitly specified.

The present-state design law is a probability measure μ on $(\mathsf{X}, \mathcal{X})$. The target transition kernel is denoted by K_0 , with density k_0 . The independent-pair observation model used for the first oracle bounds in Sections 5–5.7 is

$$X_i \sim \mu, \quad Y_i | X_i \sim K_0(X_i, \cdot), \quad i = 1, \dots, n,$$

with the pairs (X_i, Y_i) independent. Section 6 gives the dynamical transfer consequences.

3.2 Reference restart law and metrics

Let ν be a probability measure dominated by λ with density $r : \mathsf{X} \rightarrow [0, \infty)$:

$$\nu(dy) = r(y) \lambda(dy).$$

The law ν does not depend on the current state. This state-independent choice is what makes the anchor below a restart kernel and yields a Doeblin minorization. For a measurable function f on $\mathsf{X} \times \mathsf{X}$, define

$$\|f\|_{2, \mu\lambda}^2 := \int f(x, y)^2 \mu(dx) \lambda(dy), \quad \|f\|_{1, \mu\lambda} := \int |f(x, y)| \mu(dx) \lambda(dy).$$

For a bounded measurable f on $\mathsf{X} \times \mathsf{X}$, write

$$\|f\|_\infty := \sup_{(x, y) \in \mathsf{X} \times \mathsf{X}} |f(x, y)|.$$

For kernels K and L , define the integrated and uniform total-variation semimetrics

$$d_{\mu, \text{TV}}(K, L) := \int \text{TV}(K(x, \cdot), L(x, \cdot)) \mu(dx),$$

$$d_{\infty, \text{TV}}(K, L) := \sup_{x \in \mathsf{X}} \text{TV}(K(x, \cdot), L(x, \cdot)).$$

If K and L have densities k and ℓ , then

$$d_{\mu, \text{TV}}(K, L) = \frac{1}{2} \|k - \ell\|_{1, \mu\lambda}.$$

Here $\text{TV}(P, Q) := \sup_{B \in \mathcal{X}} |P(B) - Q(B)|$ for probability measures on $(\mathsf{X}, \mathcal{X})$. Because X is standard Borel, \mathcal{X} is countably generated and the supremum defining total variation may be taken over a countable determining algebra. The integrated metrics describe the design distribution used for learning. The uniform metric is stronger and will be required for general path-law perturbations in Section 6. Measurability of the map $x \mapsto \text{TV}(K(x, \cdot), L(x, \cdot))$ is standard on standard Borel spaces; for completeness see Lemma 18 in Appendix A.1.

3.3 Choice of restart law and anchor strength

The restart law ν and anchor strength ε are design parameters of the chart. The theory should not be read as saying that all choices are equivalent. The restart law plays three roles at once: it is the negative class in the contrastive experiment, the lower envelope in the anchored density, and the fallback law used by the Markovization map on degenerate rows. A useful restart law should therefore be simulable, should have support on the region where transition reconstruction is desired, and should not put negligible mass on states that are important for the downstream occupancies considered in Section 6.

The anchor strength has the complementary tradeoff. Increasing ε adds more reference mass to the anchored density and improves the lower envelope $a_0(y | x) \geq \varepsilon r(y)$, which is favorable for contrastive curvature. At the same time, the inverse map divides by $1 - \varepsilon$, so reconstruction bounds carry factors such as $(1 - \varepsilon)^{-1}$ or $(1 - \varepsilon)^{-2}$. Thus ε should be treated as a genuine statistical design parameter, not as a harmless technical constant. In applications, a conservative default is to use a full-support diffuse reference, or a mixture of an empirical next-state marginal with such a diffuse reference, and to select ε using validation contrastive risk together with the invalidity diagnostics before Markovization.

4 Contrastive Doeblin Charts

Definition 1 (Restart anchor) For $\varepsilon \in (0, 1)$ and a restart law ν , the restart anchor of a Markov kernel K is the Markov kernel

$$A_{\varepsilon, \nu} K(x, B) := (1 - \varepsilon)K(x, B) + \varepsilon\nu(B), \quad x \in \mathbf{X}, B \in \mathcal{X}.$$

If K has density k and ν has density r , then $A_{\varepsilon, \nu} K$ has density

$$a_K(y | x) := (1 - \varepsilon)k(y | x) + \varepsilon r(y).$$

Theorem 2 (Contrastive Doeblin chart) Let $\varepsilon \in (0, 1)$ and let ν be a probability measure on $(\mathbf{X}, \mathcal{X})$.

(i) The image of $A_{\varepsilon, \nu}$ is exactly the class of Markov kernels A satisfying

$$A(x, B) \geq \varepsilon\nu(B), \quad x \in \mathbf{X}, B \in \mathcal{X}.$$

For such an A , the inverse kernel is

$$A_{\varepsilon, \nu}^{-1} A(x, B) = \frac{A(x, B) - \varepsilon\nu(B)}{1 - \varepsilon}.$$

(ii) For all Markov kernels K and L ,

$$d_{\mu, \text{TV}}(A_{\varepsilon, \nu} K, A_{\varepsilon, \nu} L) = (1 - \varepsilon)d_{\mu, \text{TV}}(K, L)$$

for every design law μ , and

$$d_{\infty, \text{TV}}(A_{\varepsilon, \nu} K, A_{\varepsilon, \nu} L) = (1 - \varepsilon)d_{\infty, \text{TV}}(K, L).$$

(iii) Suppose now that $\nu(dy) = r(y)\lambda(dy)$ with $r(y) > 0$ for λ -almost every y , and that A has a chosen jointly measurable density representative $a(y | x)$. Fix a contrastive ratio $\tau > 0$ and define the posterior coordinate

$$\eta_{A,a}(x, y) := \begin{cases} \frac{a(y | x)}{a(y | x) + \tau r(y)}, & r(y) > 0, \\ 0, & r(y) = 0 \end{cases}$$

on $X \times X$. Then a is recovered from $\eta_{A,a}$ on the set where $r(y) > 0$ by

$$a(y | x) = \tau r(y) \frac{\eta_{A,a}(x, y)}{1 - \eta_{A,a}(x, y)}.$$

If $A = A_{\varepsilon, \nu}K$, then the density of K is recovered on the same set by

$$k(y | x) = \frac{\tau r(y)\eta_{A,a}(x, y)/(1 - \eta_{A,a}(x, y)) - \varepsilon r(y)}{1 - \varepsilon}$$

Consequently, these density equalities hold $\mu \otimes \lambda$ -almost everywhere for every design law μ .

The proof of Theorem 2 is given in Appendix A.2.

Remark 3 (Anchor tradeoff and selection) *The anchor is stabilizing in the forward coordinate and amplifying in the inverse coordinate. If \hat{a} is an anchored density score and $\tilde{k}_{\hat{a}} = (\hat{a} - \varepsilon r)/(1 - \varepsilon)$, then*

$$\left\| \tilde{k}_{\hat{a}} - k_0 \right\|_{p, \mu\lambda} = \frac{1}{1 - \varepsilon} \|\hat{a} - a_0\|_{p, \mu\lambda}, \quad p \in \{1, 2\}.$$

Larger ε supplies more restart mass to the positive contrastive density, but the inverse map becomes unstable as $\varepsilon \uparrow 1$. Reference support improves the next-state contrastive coordinate; it does not by itself imply present-state occupancy coverage. In applications, ν and ε should therefore be treated as design parameters, with ε selected by validation contrastive risk and pre-Markovization invalidity diagnostics.

Kernel identities in parts (i) and (ii) are pointwise in x and in measurable sets B . Density and posterior identities in part (iii) concern chosen jointly measurable density representatives and the derived coordinate $\eta_{A,a}$; they are asserted almost everywhere.

5 Risk Geometry, Oracle Learning, and Kernel Reconstruction

This section advances the first two links in the main chain:

$$\text{contrastive risk} \Rightarrow \text{anchored density} \Rightarrow \text{valid Markov kernel}.$$

We first define the augmented contrastive risk and estimator, then state the risk geometry theorem, the oracle inequalities, and the Markovization result.

5.1 Augmented transition pairs and empirical risk

Write

$$a_0(y | x) := (1 - \varepsilon)k_0(y | x) + \varepsilon r(y)$$

for the anchored target density. To estimate a_0 from samples of K_0 , we simulate restart variables

$$\tilde{Y}_i \sim \nu, \quad Z_{ij} \sim \nu, \quad j = 1, \dots, \tau,$$

independently of the observed pairs and of each other. In the empirical construction below τ is a positive integer. The variable \tilde{Y}_i supplies the anchored positive reference mass, while the variables Z_{ij} supply negative reference draws. The current state is kept at X_i in all terms. This implementation has expectation equal to a binary experiment whose positive conditional density is $a_0(\cdot | X_i)$ and whose negative conditional density is r .

In the statistical results the contrastive ratio τ is a fixed positive integer. For any measurable candidate $a : \mathsf{X} \times \mathsf{X} \rightarrow (0, \infty)$ define

$$\eta_a(x, y) := \frac{a(y | x)}{a(y | x) + \tau r(y)},$$

and the log-loss terms

$$\ell_a^+(x, y) := -\log \eta_a(x, y), \quad \ell_a^-(x, y) := -\log(1 - \eta_a(x, y)).$$

The population risk is

$$\mathcal{R}(a) := (1 - \varepsilon)\mathbb{E}[\ell_a^+(X, Y)] + \varepsilon\mathbb{E}[\ell_a^+(X, \tilde{Y})] + \tau\mathbb{E}[\ell_a^-(X, Z)], \quad (1)$$

where $X \sim \mu$, $Y | X \sim K_0(X, \cdot)$, and $\tilde{Y}, Z \sim \nu$ are independent of X . Equivalently,

$$\mathcal{R}(a) = \int_{\mathsf{X} \times \mathsf{X}} \left[-a_0(y | x) \log \frac{a(y | x)}{a(y | x) + \tau r(y)} - \tau r(y) \log \frac{\tau r(y)}{a(y | x) + \tau r(y)} \right] \mu(dx) \lambda(dy). \quad (2)$$

The losses and risks are understood as extended-real quantities with $-\log 0 = +\infty$. Under Assumptions 4 and 5 below, all risk values used in the theorems are finite. Given observations and simulated references, the empirical risk is

$$\widehat{\mathcal{R}}_n(a) := \frac{1}{n} \sum_{i=1}^n \left[(1 - \varepsilon)\ell_a^+(X_i, Y_i) + \varepsilon\ell_a^+(X_i, \tilde{Y}_i) + \sum_{j=1}^{\tau} \ell_a^-(X_i, Z_{ij}) \right]. \quad (3)$$

By construction, $\mathbb{E}\widehat{\mathcal{R}}_n(a) = \mathcal{R}(a)$ whenever the expectation is finite.

5.2 Assumptions

Assumption 4 (Reference and target bounds) *There are constants $0 < r_- \leq r_+ < \infty$ and $M_0 < \infty$ such that*

$$r_- \leq r(y) \leq r_+ \quad \text{for every } y \in \mathsf{X}, \quad 0 \leq k_0(y | x) \leq M_0$$

for $\mu \otimes \lambda$ -almost every (x, y) .

Assumption 5 (Candidate bounds) *There are constants $0 < \gamma \leq \Gamma < \infty$ such that every $a \in \mathcal{A}_n$ is jointly measurable and satisfies*

$$\gamma \leq a(y | x) \leq \Gamma$$

for every $(x, y) \in \mathsf{X} \times \mathsf{X}$.

Assumption 4 implies

$$\varepsilon r_- \leq a_0(y | x) \leq (1 - \varepsilon)M_0 + \varepsilon r_+$$

almost everywhere. The lower bound is supplied by the restart anchor even if the original transition density vanishes.

5.3 Estimator and reconstruction procedure

Let \mathcal{A}_n be a class of positive jointly measurable candidate functions. For an optimization tolerance $\delta_{\text{opt}} \geq 0$, an anchored empirical estimator is any measurable $\hat{a}_n \in \mathcal{A}_n$ satisfying

$$\widehat{\mathcal{R}}_n(\hat{a}_n) \leq \inf_{a \in \mathcal{A}_n} \widehat{\mathcal{R}}_n(a) + \delta_{\text{opt}}.$$

The direct de-anchored density score is

$$\tilde{k}_n(y | x) := \frac{\hat{a}_n(y | x) - \varepsilon r(y)}{1 - \varepsilon}.$$

If \hat{a}_n lies in the image of the anchor map, then \tilde{k}_n is already a transition density. For general function classes it may be signed or may fail to integrate to one. Theorem 9 below gives a measurable Markovization operator that restores a valid kernel with a controlled L^1 loss.

Algorithm 1 summarizes this estimator-to-kernel conversion. The display is meant to fix the order of the three operations used in the theory: simulate the restart draws that define the empirical contrastive risk, fit an anchored score by ERM, and only then apply the deterministic de-anchoring and Markovization maps. Thus the output of the statistical step is a score \hat{a}_n , while the output used for dynamics is the valid kernel \widehat{K}_n .

5.4 Risk Geometry of the Anchored Contrastive Chart

For positive measurable a for which the risks are finite, set

$$\mathcal{E}(a) := \mathcal{R}(a) - \mathcal{R}(a_0).$$

Also define the integrated Hellinger-type discrepancy

$$H_{\mu\lambda}^2(a, a_0) := \int_{\mathsf{X} \times \mathsf{X}} \left(\sqrt{a(y | x)} - \sqrt{a_0(y | x)} \right)^2 \mu(\mathrm{d}x) \lambda(\mathrm{d}y).$$

Theorem 6 (Risk Geometry of the Anchored Contrastive Chart) *Suppose Assumptions 4 and 5 hold. Then:*

Algorithm 1 Anchored contrastive estimation and reconstruction

Require: Transition pairs $(X_i, Y_i)_{i=1}^n$; simulable restart law ν with density r ; anchor strength ε ; number of negatives τ ; candidate class \mathcal{A}_n ; optimization tolerance δ_{opt} .

Ensure: Markov transition kernel estimator \widehat{K}_n .

- 1: // **Step 1: Sample anchor positives and reference negatives**
- 2: **for** $i = 1$ **to** n **do**
- 3: Draw $\widetilde{Y}_i \sim \nu$ independently of (X_i, Y_i) .
- 4: Draw $Z_{i1}, \dots, Z_{i\tau} \stackrel{\text{i.i.d.}}{\sim} \nu$ independently of all observed and anchor-positive variables.
- 5: **end for**
- 6: // **Step 2: Fit the anchored contrastive score**
- 7: Choose a measurable $\widehat{a}_n \in \mathcal{A}_n$ satisfying

$$\widehat{\mathcal{R}}_n(\widehat{a}_n) \leq \inf_{a \in \mathcal{A}_n} \widehat{\mathcal{R}}_n(a) + \delta_{\text{opt}}.$$

- 8: // **Step 3: De-anchor and Markovize**
- 9: Set

$$\widetilde{k}_n(y | x) \leftarrow \frac{\widehat{a}_n(y | x) - \varepsilon r(y)}{1 - \varepsilon}.$$

- 10: Set $\widehat{k}_n \leftarrow \mathfrak{M}\widetilde{k}_n$.
- 11: Set $\widehat{K}_n(x, dy) \leftarrow \widehat{k}_n(y | x)\lambda(dy)$.
- 12: **return** \widehat{K}_n .

(i) **Identification.** The anchored target density a_0 uniquely minimizes \mathcal{R} over all positive measurable a for which the risk in (2) is finite, up to $\mu \otimes \lambda$ -almost-everywhere equality.

(ii) **L^2 calibration.** There exist constants $0 < c_- \leq c_+ < \infty$, depending only on $(\varepsilon, \tau, r_-, r_+, M_0, \gamma, \Gamma)$, such that for every $a \in \mathcal{A}_n$,

$$c_- \|a - a_0\|_{2, \mu\lambda}^2 \leq \mathcal{E}(a) \leq c_+ \|a - a_0\|_{2, \mu\lambda}^2.$$

Consequently,

$$\left\| \widetilde{k}_a - k_0 \right\|_{2, \mu\lambda}^2 \leq \frac{1}{(1 - \varepsilon)^2 c_-} \mathcal{E}(a),$$

where $\widetilde{k}_a := (a - \varepsilon r)/(1 - \varepsilon)$.

(iii) **Contrastive KL representation.** Writing $\eta_0(x, y) := a_0(y | x)/\{a_0(y | x) + \tau r(y)\}$, the excess risk has the exact representation

$$\mathcal{E}(a) = \int_{\mathcal{X} \times \mathcal{X}} (a_0(y | x) + \tau r(y)) \text{KL}(\text{Ber}(\eta_0(x, y)) \| \text{Ber}(\eta_a(x, y))) \mu(dx) \lambda(dy). \quad (4)$$

(iv) **L^1 and Hellinger consequences.**

$$\|a - a_0\|_{1, \mu\lambda}^2 \leq c_-^{-1} \mathcal{E}(a), \quad (5)$$

$$H_{\mu\lambda}^2(a, a_0) \leq \frac{1}{4m_a c_-} \mathcal{E}(a), \quad m_a := \min\{\varepsilon r_-, \gamma\}. \quad (6)$$

If a is itself a transition density and $A_a(x, dy) = a(y | x)\lambda(dy)$, then

$$d_{\mu, \text{TV}}(A_a, A_{\varepsilon, \nu}K_0)^2 \leq \frac{1}{4c_-} \mathcal{E}(a).$$

The proof of Theorem 6 is given in Appendix A.3. The uniform boundedness assumptions keep the curvature and concentration statements global; tail-localized extensions would require standard truncation arguments (Wainwright, 2019).

5.5 Oracle Inequalities for Anchored Contrastive ERM

To formally analyze the statistical properties of our estimator, it is mathematically convenient to package the interdependent sample components from Section 3 into a single independent observation block. Specifically, for a block

$$B = (X, Y, \tilde{Y}, Z_1, \dots, Z_\tau)$$

distributed as described previously, define

$$g_a(B) := (1 - \varepsilon)\ell_a^+(X, Y) + \varepsilon\ell_a^+(X, \tilde{Y}) + \sum_{j=1}^{\tau} \ell_a^-(X, Z_j).$$

Let $\mathcal{G}_n := \{g_a : a \in \mathcal{A}_n\}$. In this block-based notation, the empirical and population contrastive risks are precisely the sample average and expectation of this block-wise loss, respectively:

$$\widehat{\mathcal{R}}_n(a) := \frac{1}{n} \sum_{i=1}^n g_a(B_i), \quad \mathcal{R}(a) := \mathbb{E}[g_a(B)].$$

Throughout this subsection, the blocks B_1, \dots, B_n are independent copies of B unless a different sampling scheme is stated explicitly. Set the expected uniform deviation as

$$\Delta_n := \mathbb{E} \sup_{a \in \mathcal{A}_n} \left| \widehat{\mathcal{R}}_n(a) - \mathcal{R}(a) \right|.$$

We assume that the displayed supremum is measurable. Equivalently, each expectation in Theorem 7 may be read as an outer expectation.

For a class \mathcal{A} of functions on $\mathsf{X} \times \mathsf{X}$ and $\delta > 0$, write $N_\infty^{\text{int}}(\delta, \mathcal{A})$ for the internal sup-norm covering number: it is the smallest N for which there exist $a_1, \dots, a_N \in \mathcal{A}$ such that

$$\sup_{a \in \mathcal{A}} \min_{j=1, \dots, N} \|a - a_j\|_\infty \leq \delta.$$

Theorem 7 (Oracle Inequalities for Anchored Contrastive ERM) *Under Assumptions 4 and 5, let \widehat{a}_n be a measurable δ_{opt} -approximate empirical risk minimizer over \mathcal{A}_n . Then:*

(i) **Global oracle bound.**

$$\mathbb{E} \left\| \widetilde{k}_{\widehat{a}_n} - k_0 \right\|_{2, \mu\lambda}^2 \leq \frac{2\Delta_n + \delta_{\text{opt}}}{(1 - \varepsilon)^2 c_-} + \frac{c_+}{(1 - \varepsilon)^2 c_-} \inf_{a \in \mathcal{A}_n} \|a - a_0\|_{2, \mu\lambda}^2,$$

where c_- and c_+ are the calibration constants in Theorem 6. Here, the expected uniform deviation Δ_n can be explicitly upper-bounded for any $\delta > 0$ by

$$\Delta_n \leq 2L_\ell\delta + B_\ell\sqrt{\frac{2\log(2N_\infty^{\text{int}}(\delta, \mathcal{A}_n))}{n}},$$

where $N_\infty^{\text{int}}(\delta, \mathcal{A}_n) = N_\infty^{\text{int}}(\delta, \mathcal{A}_n)$ is the internal sup-norm covering number defined above.

(ii) **Bernstein geometry.** There exist finite constants V_ℓ and B_h , depending only on $(\varepsilon, \tau, r_-, r_+, M_0, \gamma, \Gamma)$, such that for every $a \in \mathcal{A}_n$,

$$\mathbb{E} \left[(g_a(B) - g_{a_0}(B))^2 \right] \leq V_\ell \mathcal{E}(a), \quad |g_a(B) - g_{a_0}(B)| \leq B_h \text{ a.s.}$$

Here the blocks $(B_i)_{i=1}^n$ are i.i.d.

(iii) **Localized fast-rate oracle bound.** Let $\delta > 0$ and $N := N_\infty^{\text{int}}(\delta, \mathcal{A}_n) < \infty$. Put $u := \log(2N) + \log(2/\eta)$ for $\eta \in (0, 1)$. There is a constant $C_{\text{fast}} < \infty$, depending only on $(\varepsilon, \tau, r_-, r_+, M_0, \gamma, \Gamma)$, such that with probability at least $1 - \eta$,

$$\mathcal{E}(\hat{a}_n) \leq \frac{5}{3} \inf_{a \in \mathcal{A}_n} \mathcal{E}(a) + C_{\text{fast}} \left[L_\ell\delta + \delta_{\text{opt}} + \frac{\log\{2N_\infty^{\text{int}}(\delta, \mathcal{A}_n)/\eta\}}{n} \right], \quad (7)$$

Consequently, on the same event,

$$\left\| \tilde{k}_{\hat{a}_n} - k_0 \right\|_{2, \mu\lambda}^2 \leq \frac{C_{\text{fast}}}{(1 - \varepsilon)^2 c_-} \left[\inf_{a \in \mathcal{A}_n} \mathcal{E}(a) + L_\ell\delta + \delta_{\text{opt}} + \frac{\log\{2N_\infty^{\text{int}}(\delta, \mathcal{A}_n)/\eta\}}{n} \right].$$

The proof of Theorem 7 is given in Appendix A.4.

5.6 Valid-Kernel Reconstruction by Markovization

The next theorem is deterministic. It clarifies how a de-anchored score can be converted to a Markov kernel without asserting that every positive network score lies in the anchor image.

Definition 8 (Markovization) Let $g : \mathcal{X} \times \mathcal{X} \rightarrow \mathbb{R}$ be jointly measurable and assume $\int |g(y | x)| \lambda(\text{d}y) < \infty$ for every x . Write $g^+(y | x) = \max\{g(y | x), 0\}$ and $c_g(x) = \int g^+(y | x) \lambda(\text{d}y)$. Define

$$\mathfrak{M}g(y | x) := \begin{cases} g^+(y | x)/c_g(x), & c_g(x) > 0, \\ r(y), & c_g(x) = 0. \end{cases}$$

Theorem 9 (Valid-Kernel Reconstruction by Markovization) The function $\mathfrak{M}g$ in Definition 8 is a jointly measurable transition density. For every transition density k ,

$$\int |\mathfrak{M}g(y | x) - k(y | x)| \lambda(\text{d}y) \leq 2 \int |g(y | x) - k(y | x)| \lambda(\text{d}y) \quad \text{for every } x.$$

Consequently,

$$\|\mathfrak{M}g - k\|_{1,\mu\lambda} \leq 2 \|g - k\|_{1,\mu\lambda}.$$

In particular, on the event of Theorem 7(iii), the Markovized de-anchored estimator

$$\widehat{k}_n := \mathfrak{M}\widetilde{k}_{\widehat{a}_n}, \quad \widehat{K}_n(x, dy) := \widehat{k}_n(y | x)\lambda(dy)$$

satisfies

$$d_{\mu,\text{TV}}(\widehat{K}_n, K_0)^2 \leq \frac{C_{\text{fast}}}{(1-\varepsilon)^2 c_-} \left[\inf_{a \in \mathcal{A}_n} \mathcal{E}(a) + L_\ell \delta + \delta_{\text{opt}} + \frac{\log(2N_\infty^{\text{int}}(\delta, \mathcal{A}_n)) + \log(2/\eta)}{n} \right]. \quad (8)$$

The bound is in integrated total variation for the valid kernel \widehat{K}_n ; we do not claim that Markovization preserves squared $L^2(\mu \otimes \lambda)$ error.

The proof of Theorem 9 is given in Appendix A.5.

5.7 Hölder–ReLU Rate and Minimax Near-Optimality

We now instantiate the oracle theory in a standard nonparametric regime. The transition density $k_0(y | x)$ is viewed as a function on $[0, 1]^d \times [0, 1]^d$, hence the effective dimension is $2d$. Under a Hölder smoothness condition and a clipped ReLU approximation–entropy hypothesis, the anchored contrastive estimator attains the usual nonparametric rate

$$n^{-2\beta/(2\beta+2d)}$$

up to logarithmic factors. The same rate transfers to the Markovized kernel in integrated total variation. The minimax lower bound below shows that the squared $L^2(\mu \otimes \lambda)$ rate is optimal up to logarithmic factors. Throughout this section, set

$$\bar{d} := 2d.$$

Assumption 10 (Hölder–ReLU approximation and entropy) *Let $\mathsf{X} = \mathsf{Y} = [0, 1]^d$, and let λ be Lebesgue probability measure on Y . For every integer $S \geq 2$, there is a clipped ReLU class $\mathcal{A}(S)$ with values in $[\gamma, \Gamma]$, consisting of jointly measurable functions on $\mathsf{X} \times \mathsf{Y}$, such that the following holds.*

For every fixed Hölder radius $R > 0$, there exist constants $C_{\text{app}}(R), C_{\text{ent}}(R) < \infty$ and $\kappa_{\text{app}}, \kappa_{\text{ent}} \geq 0$ such that, whenever $a_0 \in \mathcal{H}_d^\beta(R)$ and

$$\gamma \leq \varepsilon r_-, \quad \Gamma \geq (1 - \varepsilon)M_0 + \varepsilon r_+,$$

we have, for all $S \geq 2$ and all $n \geq 3$,

$$\inf_{a \in \mathcal{A}(S)} \|a - a_0\|_\infty \leq C_{\text{app}}(R) S^{-\beta/\bar{d}} (\log S)^{\kappa_{\text{app}}},$$

$$\log N_\infty^{\text{int}}(n^{-1}, \mathcal{A}(S)) \leq C_{\text{ent}}(R) S (\log n)^{\kappa_{\text{ent}}}.$$

Here N_∞^{int} denotes the internal sup-norm covering number.

For $\beta > 0$, $R > 1$, and $0 < m < 1 < M$, let $\mathcal{K}_\beta(R, m, M)$ denote the class of transition densities $k(y | x)$ on $[0, 1]^d \times [0, 1]^d$ such that

$$k \in \mathcal{H}_d^\beta(R), \quad m \leq k(y | x) \leq M, \quad \int_{[0,1]^d} k(y | x) \lambda(dy) = 1 \quad \text{for every } x.$$

We now state the concrete rate consequence. The upper bound is formulated for the anchored contrastive estimator over the clipped ReLU sieve from Assumption 10. The minimax comparison is stated over the following standard bounded Hölder class of transition densities.

Theorem 11 (Hölder–ReLU Rate and Minimax Near-Optimality) *Let $X = [0, 1]^d$ and suppose the bounded reference/target regime of Assumption 4 holds. Assume also that Assumption 10 holds for the anchored target density a_0 . Let \hat{a}_n be a measurable δ_{opt} -approximate empirical risk minimizer over the clipped ReLU sieve*

$$\mathcal{A}_n := \mathcal{A}(S_n), \quad S_n := \left\lceil n^{\bar{d}/(2\beta + \bar{d})} \right\rceil,$$

and define the de-anchored and Markovized estimators

$$\tilde{k}_n := \frac{\hat{a}_n - \varepsilon r}{1 - \varepsilon}, \quad \hat{k}_n := \mathfrak{M} \tilde{k}_n, \quad \hat{K}_n(x, dy) := \hat{k}_n(y | x) \lambda(dy).$$

Then there are constants $C, \kappa < \infty$ such that for all $n \geq 3$ and $\eta \in (0, 1)$, with probability at least $1 - \eta$,

$$\left\| \tilde{k}_n - k_0 \right\|_{2, \mu\lambda}^2 \vee d_{\mu, \text{TV}}(\hat{K}_n, K_0)^2 \leq C \left[n^{-2\beta/(2\beta + 2d)} (\log n)^\kappa + \delta_{\text{opt}} + \frac{\log(1/\eta)}{n} \right].$$

Moreover, when $\mu = \lambda$ is Lebesgue probability measure on $[0, 1]^d$, for every $\beta > 0$, $R > 1$, and $0 < m < 1 < M$, the minimax risk over the bounded Hölder transition-density class $\mathcal{K}_\beta(R, m, M)$ satisfies

$$\inf_{\hat{k}} \sup_{K \in \mathcal{K}_\beta(R, m, M)} \mathbb{E}_K \left\| \hat{k} - k \right\|_{2, \mu\lambda}^2 \geq c n^{-2\beta/(2\beta + 2d)}$$

for a constant $c > 0$. Hence the squared $L^2(\mu \otimes \lambda)$ rate is minimax near-optimal up to logarithmic factors. The squared TV upper bound follows from the same estimator and the Markovization argument, but no separate TV minimax lower bound is claimed.

The proof of Theorem 11 is given in Appendix A.6. Assumption 10 is a standard ReLU approximation–entropy input rather than a new neural approximation theorem; see, for example, Yarotsky (2017).

6 Dynamic Transfer

This section closes the loop

contrastive risk \Rightarrow anchored density \Rightarrow valid Markov kernel \Rightarrow dynamical error control.

We give the finite-horizon transfer theorem from learned kernel error to marginal, path-law, and occupation-measure error under an explicit occupancy coverage condition. A final proposition shows why such a coverage assumption is unavoidable.

6.1 From Contrastive Excess Risk to Finite-Horizon Dynamics

Theorem 12 (From Contrastive Excess Risk to Finite-Horizon Dynamics) *Let K_0 be the target kernel and let \hat{a} be a learned anchored score with $\gamma \leq \hat{a} \leq \Gamma$. Form the valid learned kernel \hat{K} by de-anchoring and Markovization as in Theorem 9. Fix an initial law ξ and a horizon $T \in \mathbb{N}$. For any two Markov kernels K and L , define the pointwise kernel error*

$$e_{K,L}(x) := \text{TV}(K(x, \cdot), L(x, \cdot)).$$

For the learned-kernel application, write $e(x) := e_{K_0, \hat{K}}(x)$.

For any Markov kernels K and L and any $m \leq T$, the occupancy-weighted perturbation bound (Theorem 21 in Appendix A.7) gives

$$\text{TV}(\xi K^m, \xi L^m) \leq \sum_{s=0}^{m-1} \int e_{K,L}(x) (\xi K^s)(dx). \quad (9)$$

The same right-hand side bounds the total-variation distance between the length- m path laws and the normalized length- m occupation measures $\bar{\Gamma}_m^K := \frac{1}{m} \sum_{s=0}^{m-1} \xi K^s$.

Assume the occupancy coverage condition: for each $s = 0, \dots, T-1$,

$$\xi K_0^s \ll \mu, \quad C_s := \text{ess sup}_{\mu} \frac{d(\xi K_0^s)}{d\mu} < \infty.$$

Then for every $m \leq T$:

(i) **L^1 -coverage bound.**

$$\text{TV}(\xi K_0^m, \xi \hat{K}^m) \leq \left(\sum_{s=0}^{m-1} C_s \right) d_{\mu, \text{TV}}(K_0, \hat{K}).$$

(ii) **L^2 -coverage bound.** With $C_{\xi, \mu, m} := \max_{0 \leq s < m} C_s$,

$$\text{TV}(\xi K_0^m, \xi \hat{K}^m) \leq m \sqrt{C_{\xi, \mu, m}} \|e\|_{L^2(\mu)}.$$

(iii) **Normalized occupation measures.** Write the normalized occupation measure $\bar{\Gamma}_m^K := \frac{1}{m} \sum_{s=0}^{m-1} \xi K^s$. Then

$$\text{TV}(\bar{\Gamma}_m^{K_0}, \bar{\Gamma}_m^{\hat{K}}) \leq \frac{m-1}{2} \sqrt{C_{\xi, \mu, m}} \|e\|_{L^2(\mu)}.$$

By Theorem 9, $e(x) \leq \int \left| \tilde{k}_{\hat{a}}(y | x) - k_0(y | x) \right| \lambda(dy)$ pointwise, and Cauchy-Schwarz gives $\|e\|_{L^2(\mu)} \leq \left\| \tilde{k}_{\hat{a}} - k_0 \right\|_{L^2(\mu \otimes \lambda)}$. Finally, the L^2 calibration in Theorem 6 yields

$$\left\| \tilde{k}_{\hat{a}} - k_0 \right\|_{L^2(\mu \otimes \lambda)}^2 \leq \frac{1}{(1-\varepsilon)^2 c_-} \mathcal{E}(\hat{a}).$$

Combining these steps, contrastive excess risk transfers directly to finite-horizon dynamical error:

$$\mathrm{TV}(\xi K_0^m, \xi \widehat{K}^m) \leq \frac{m\sqrt{C_{\xi,\mu,m}}}{(1-\varepsilon)\sqrt{c_-}} \mathcal{E}(\widehat{a})^{1/2},$$

and the normalized occupation measures $\bar{\Gamma}_m^{K_0}$ and $\bar{\Gamma}_m^{\widehat{K}}$ satisfy the same inequality with the factor m replaced by $(m-1)/2$, as in part (iii).

The proof of Theorem 12 is given in Appendix A.7.

Remark 13 (Invariant law perturbation under contraction) *The main transfer theorem is finite-horizon and occupancy-weighted. Stationary perturbation requires stronger assumptions: if one has a uniform kernel error $d_{\infty,\mathrm{TV}}(K,L)$ and the Dobrushin coefficient*

$$\alpha(K) := \sup_{x,x'} \mathrm{TV}(K(x,\cdot), K(x',\cdot)) < 1,$$

then the standard Dobrushin contraction yields

$$\mathrm{TV}(\pi_K, \pi_L) \leq d_{\infty,\mathrm{TV}}(K,L)/(1-\alpha(K)).$$

See Corollary 22 in Appendix A.7.

6.2 Trajectory Sampling Through the Same Reconstruction Interface

The independent-pair oracle theorem isolates the contrastive geometry most cleanly. For trajectory data, temporal dependence affects the statistical oracle step but not the reconstruction interface. We record a conservative thinning-and-coupling extension. Its purpose is not to optimize dependent-data rates, but to show that de-anchoring, Markovization, and finite-horizon perturbation remain unchanged once a trajectory oracle bound is available.

Let $(X_t)_{t \geq 0}$ be a stationary Markov chain with invariant law μ and transition kernel K_0 . Its absolute-regularity coefficients are

$$\beta_X(s) := \sup_{t \geq 0} \beta(\sigma(X_0, \dots, X_t), \sigma(X_{t+s}, X_{t+s+1}, \dots)).$$

Fix an integer $q \geq 2$ and write $M := \lfloor N/q \rfloor$. Assume $M \geq 1$. From a trajectory X_0, \dots, X_N , retain only

$$(X_{jq-1}, X_{jq}), \quad j = 1, \dots, M.$$

For each retained transition, draw $\widetilde{Y}_j \sim \nu$ and $Z_{j1}, \dots, Z_{j\tau} \stackrel{\text{i.i.d.}}{\sim} \nu$ independently of the trajectory and of all other auxiliary variables, and set

$$B_j^{(q)} := (X_{jq-1}, X_{jq}, \widetilde{Y}_j, Z_{j1}, \dots, Z_{j\tau}).$$

The thinned trajectory empirical risk is

$$\widehat{\mathcal{R}}_{M,q}^{\mathrm{tr}}(a) := \frac{1}{M} \sum_{j=1}^M g_a(B_j^{(q)}).$$

Theorem 14 (Trajectory sampling through the reconstruction interface) *Suppose Assumptions 4 and 5 hold. Let $\widehat{a}_{M,q}^{\text{tr}}$ be a measurable δ_{opt} -approximate minimizer of $\widehat{\mathcal{R}}_{M,q}^{\text{tr}}$ over \mathcal{A}_M . Let $\eta \in (0, 1)$ and assume*

$$(M - 1)\beta_X(q - 1) \leq \eta/2.$$

For every $\delta > 0$ with $N_\infty^{\text{int}}(\delta, \mathcal{A}_M) < \infty$, there are constants $C_{\text{or}}, C_{\text{ker}}, C_{\text{dyn}} < \infty$, depending only on $(\varepsilon, \tau, r_-, r_+, M_0, \gamma, \Gamma)$, such that with probability at least $1 - \eta$,

$$\mathcal{E}(\widehat{a}_{M,q}^{\text{tr}}) \leq C_{\text{or}} \mathfrak{R}_{M,q}(\eta, \delta),$$

where

$$\mathfrak{R}_{M,q}(\eta, \delta) := \inf_{a \in \mathcal{A}_M} \mathcal{E}(a) + L_\ell \delta + \delta_{\text{opt}} + \frac{\log\{4N_\infty^{\text{int}}(\delta, \mathcal{A}_M)/\eta\}}{M}.$$

Define

$$\widetilde{k}_{M,q}^{\text{tr}} := \frac{\widehat{a}_{M,q}^{\text{tr}} - \varepsilon r}{1 - \varepsilon}, \quad \widehat{k}_{M,q}^{\text{tr}} := \mathfrak{M} \widetilde{k}_{M,q}^{\text{tr}},$$

and let $\widehat{K}_{M,q}^{\text{tr}}(x, dy) := \widehat{k}_{M,q}^{\text{tr}}(y | x)\lambda(dy)$. Then

$$d_{\mu, \text{TV}}(\widehat{K}_{M,q}^{\text{tr}}, K_0)^2 \leq C_{\text{ker}} \mathfrak{R}_{M,q}(\eta, \delta).$$

If the occupancy coverage condition of Theorem 12 holds up to horizon T , then for every integer $1 \leq h \leq T$,

$$\text{TV}\left(\xi K_0^h, \xi(\widehat{K}_{M,q}^{\text{tr}})^h\right) \leq h\sqrt{C_{\varepsilon, \mu, h} C_{\text{dyn}}} \mathfrak{R}_{M,q}(\eta, \delta)^{1/2}.$$

The same right-hand side also bounds the total-variation distance between the corresponding length- h path laws. The normalized occupation-measure bound holds with h replaced by $(h - 1)/2$.

The proof of Theorem 14 is given in Appendix A.8.

Corollary 15 (Geometrically mixing trajectories) *Suppose, in addition to the assumptions of Theorem 14, that*

$$\beta_X(s) \leq B\rho^s, \quad 0 < B < \infty, \quad 0 < \rho < 1.$$

For

$$q_{N,\eta} := \max\left\{2, 1 + \left\lceil \frac{\log(2BN/\eta)}{|\log \rho|} \right\rceil\right\}, \quad N_{\text{eff}} := \left\lfloor \frac{N}{q_{N,\eta}} \right\rfloor,$$

and $N_{\text{eff}} \geq 1$, the conclusions of Theorem 14 hold with $q = q_{N,\eta}$ and $M = N_{\text{eff}}$. In particular, $N_{\text{eff}} \asymp N/\log(N/\eta)$ as N/η grows, up to constants depending on (B, ρ) .

The proof of Corollary 15 is given in Appendix A.9.

Under the Hölder–ReLU assumptions of Theorem 11, the same substitution gives, when the sieve is tuned to the retained sample size,

$$d_{\mu, \text{TV}}(\widehat{K}_{M,q}^{\text{tr}}, K_0)^2 \lesssim M^{-2\beta/(2\beta+2d)} (\log M)^\kappa.$$

For geometrically β -mixing trajectories with the choice in Corollary 15, this becomes

$$d_{\mu, \text{TV}}(\widehat{K}_{N_{\text{eff}}, qN, \eta}^{\text{tr}}, K_0)^2 \lesssim N^{-2\beta/(2\beta+2d)} (\log N)^{\kappa'}$$

for some $\kappa' > 0$. Thus geometric temporal dependence changes the logarithmic factor but not the main nonparametric exponent.

Remark 16 (Statistical anchoring versus restart-controlled data collection) *The geometric β -mixing assumption is imposed on the observational chain with kernel K_0 . The Doeblin anchor used in the statistical chart does not by itself make that trajectory geometrically mixing, because the data are sampled from K_0 , not from $A_{\varepsilon, \nu} K_0$.*

If data collection is instead actively restart-controlled and the observed trajectory is generated by $A_{\varepsilon, \nu} K_0$, then the Doeblin minorization provides an explicit geometric mixing mechanism. This is a different sampling design: the empirical contrastive construction must be adjusted accordingly, since the observed positive transitions are already sampled from the anchored kernel.

6.3 A limitation example

Proposition 17 (Integrated design error need not control stationarity) *For every $\rho \in (0, 1/2)$ there exist two irreducible Markov kernels K_ρ and L_ρ on the two-point space $\{0, 1\}$ and a design law μ_ρ such that*

$$d_{\mu_\rho, \text{TV}}(K_\rho, L_\rho) \leq \rho$$

while their invariant laws satisfy

$$\text{TV}(\pi_{K_\rho}, \pi_{L_\rho}) \geq \frac{1}{4}.$$

The proof of Proposition 17 is given in Appendix A.10.

This example shows that the occupancy coverage assumption in Theorem 12 is not merely a technical convenience: an integrated learning error under a design law without sufficient coverage is not automatically a guarantee about stationary behavior. The obstruction appears already in a two-point state space.

7 Two Diagnostic Examples

The following finite-state examples use probability masses directly. Equivalently, the dominating measure is counting measure on the displayed finite state space, so a kernel density is just a transition probability mass.

7.1 A sparse two-state chart

Let $\mathsf{X} = \{0, 1\}$, let $\nu = (1/2, 1/2)$, and consider the deterministic flip chain

$$K_0(0, \cdot) = \delta_1, \quad K_0(1, \cdot) = \delta_0, \quad K_0 = \begin{pmatrix} 0 & 1 \\ 1 & 0 \end{pmatrix}.$$

This kernel has zero transition probabilities on half of the state pairs. The anchored kernel is

$$A_{\varepsilon,\nu}K_0 = \begin{pmatrix} \varepsilon/2 & 1 - \varepsilon/2 \\ 1 - \varepsilon/2 & \varepsilon/2 \end{pmatrix}.$$

Therefore

$$A_{\varepsilon,\nu}K_0(x, \{y\}) \geq \varepsilon\nu(\{y\}) = \varepsilon/2, \quad x, y \in \{0, 1\}.$$

In mass notation the contrastive risk targets

$$a_0(y | x) = (1 - \varepsilon)k_0(y | x) + \varepsilon r(y), \quad r(0) = r(1) = 1/2,$$

and the inverse chart is the entrywise affine map

$$k_0(y | x) = \frac{a_0(y | x) - \varepsilon r(y)}{1 - \varepsilon}.$$

Thus the original transition may be sparse or deterministic, while the anchored transition is strictly inside the positive cone determined by the reference law. The anchor defines a positive contrastive coordinate whose inverse recovers the original sparse kernel, at the price of the de-anchoring factor $(1 - \varepsilon)^{-1}$.

7.2 A signed de-anchored row

The affine inverse of the anchor chart is applied to an estimated score, not to the true a_0 . A de-anchored row can therefore be close in L^1 and still fail to be a probability mass. For example, suppose the target row at state 0 is deterministic,

$$k_0(0 | 0) = 1, \quad k_0(1 | 0) = 0,$$

but the de-anchored score for that row is

$$\tilde{k}(0 | 0) = 1.01, \quad \tilde{k}(1 | 0) = -0.01.$$

The row sum is one and the L^1 error on this row is

$$|1.01 - 1| + |-0.01 - 0| = 0.02,$$

but $\tilde{k}(\cdot | 0)$ is not a probability mass because it has a negative entry. Markovization clips and renormalizes:

$$(1.01, -0.01) \mapsto (1.01, 0) \mapsto (1, 0).$$

This is the finite-state picture behind Theorem 9: the learned score must be returned to the cone of Markov kernels before it is iterated.

8 Experiments

The experiments are designed as interface diagnostics rather than leaderboard benchmarks. The goal is not to claim superiority over specialized conditional density estimators, but to test whether each operation required by the theory is empirically necessary: anchoring improves the contrastive coordinate, de-anchoring targets the original kernel rather than the

anchored kernel, Markovization restores transition-kernel validity after score learning, and one-step kernel error predicts finite-horizon dynamical error under coverage. We therefore test the full pipeline

$$\hat{a}_\theta \longrightarrow \tilde{k}_\theta \longrightarrow \hat{k}_\theta = \mathfrak{M}\tilde{k}_\theta \longrightarrow d_{\mu, \text{TV}}(\hat{K}_\theta, K_0) \longrightarrow \text{finite-horizon dynamic error.}$$

Unlike the finite-state diagnostics in Section 7, the main experiments train the anchored contrastive score. The estimator is a clipped ReLU network

$$a_\theta(x, y) = \gamma + (\Gamma - \gamma)\sigma(f_\theta(x, y)),$$

trained by binary contrastive logistic loss with positive samples from the anchored transition $(1 - \varepsilon)K_0(x, \cdot) + \varepsilon\nu$ and negative samples from ν . In the public implementation this anchored positive law is represented exactly by the weighted double-positive empirical risk in (3): for each observed pair the loss includes both the data transition with weight $1 - \varepsilon$ and an independently drawn restart transition with weight ε . The network output is the bounded score a_θ itself; the contrastive classification logit is then $\log\{a_\theta(x, y)/(\tau r(y))\}$. Thus the training objective uses the same bounded candidate parametrization and weighted empirical risk as the theoretical estimator. After training, we de-anchor, Markovize, and evaluate the resulting kernel on common Monte Carlo or grid integration sets. The reproducibility repository is available at https://github.com/Ao-Xu/doesblin_exp_2026.

8.1 Protocol, models, and evaluation metrics

The synthetic models are deliberately chosen to stress different parts of the theory: smooth kernels test calibration in a regular setting; multimodal and nearly deterministic kernels test non-Gaussian and sparse transition behavior; trajectory experiments isolate temporal dependence; and rare-state chains test the necessity of occupancy coverage. The complete experiment-to-output index, synthetic model grid, and implementation parameters are recorded in the repository README for reproduction. The experiments are synthetic because the target kernel must be known in order to evaluate integrated TV, path-law TV upper bounds, and coverage failure exactly. These experiments should therefore be read as controlled diagnostics of the reconstruction chain rather than as uncontrolled real-data benchmarks. All training-based figures in this section are generated end-to-end by the public script; deterministic diagnostic examples are identified separately.

For continuous kernels, Markovization and TV integrals are evaluated by grid quadrature on common design and integration points. We report contrastive excess risk, anchored and de-anchored squared errors, integrated total variation, and the pre-Markovization invalidity diagnostics

$$\text{NegMass}(\tilde{k}_\theta) = \mathbb{E}_{X \sim \mu} \int (-\tilde{k}_\theta(y | X))_+ d\lambda(y), \quad \text{RowErr}(\tilde{k}_\theta) = \mathbb{E}_{X \sim \mu} \left| \int \tilde{k}_\theta(y | X) d\lambda(y) - 1 \right|.$$

For finite-state dynamics we compute rollout TV, occupation TV, stationary TV, and occupancy-weighted upper bounds for path-law TV directly from matrices. Unless stated otherwise, Monte Carlo summaries use ten seeds with standard-error bars. The method comparison includes the proposed pipeline, nearby ablations, and a row-normalized Gaussian conditional-density baseline evaluated on the same grids.

Component	Theory estimator	Public implementation
Positive samples	Weighted double-positive risk $(1 - \varepsilon)\ell^+(X, Y) + \varepsilon\ell^+(X, \tilde{Y})$	The same weighted double-positive construction; no Bernoulli mixture thinning is used.
Score parametrization	Bounded candidate functions $\gamma \leq a \leq \Gamma$; posterior $a/(a + \tau r)$	Bounded score network $a_\theta = \gamma + (\Gamma - \gamma)\sigma(f_\theta)$; logistic logit $\log\{a_\theta/(\tau r)\}$.
Calibration plot	Excess contrastive risk versus density error	Held-out weighted validation excess $\hat{R}_{\text{val}}(\hat{a}) - \hat{R}_{\text{val}}(a_0)$; grid density errors are oracle diagnostics.
Reference and Markovization	Restart density with lower envelope; valid-kernel repair	Matched sampler/density pairs; poor coverage is a 0.1 uniform plus 0.9 beta mixture; continuous-state integrals use grid quadrature.

Table 1: Alignment between the theoretical estimator, implemented estimator, and evaluated quantities.

8.2 End-to-end calibration of anchored contrastive learning

The first experiment tests the calibration implication

$$\mathcal{E}(a_\theta) \text{ tracks } \|a_\theta - a_0\|_{2,\mu\lambda}^2 \text{ and } \|\tilde{k}_\theta - k_0\|_{2,\mu\lambda}^2.$$

We use smooth, multimodal, and rough one-dimensional wrapped transition kernels. Each sample size and seed trains a fresh anchored contrastive network. The excess risk is evaluated on independent validation contrastive blocks, while density errors are computed on a fixed integration grid.

Figure 1 shows that validation excess risk orders the trained scores consistently with the density errors used in the theory: the log-log correlation with anchored L^2 error is about 0.94, and de-anchoring preserves this ordering up to the affine factor $(1 - \varepsilon)^{-1}$. We interpret excess risk as a model-selection proxy, not as a tight finite-sample numerical surrogate for density loss.

8.3 Valid-kernel reconstruction and Markovization

The second experiment checks whether Markovization is actually needed for learned scores. We train contrastive scores, de-anchor them, and compare the signed pre-Markovization score with the Markovized density. The key statistic is the empirical repair ratio

$$R_M = \frac{\|\mathfrak{M}\tilde{k}_\theta - k_0\|_{1,\mu}}{\|\tilde{k}_\theta - k_0\|_{1,\mu}},$$

which is bounded by 2 in Theorem 9.

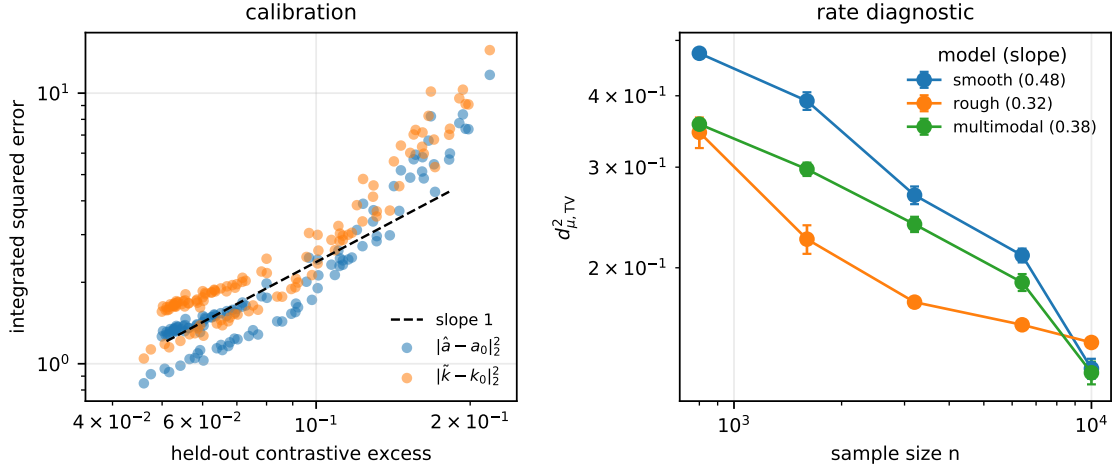


Figure 1: Statistical diagnostics for the contrastive front end. Left: end-to-end calibration, where each point is a trained neural score under one model, sample size, and seed. The log-log cloud aligns with a slope-one reference in aggregate. Right: real-trained one-dimensional rate diagnostic, with fitted slopes shown in parentheses.

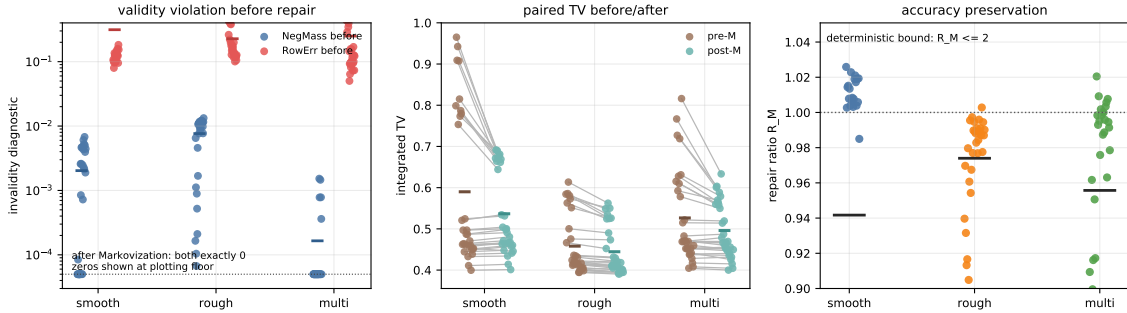


Figure 2: Markovization repairs validity without amplifying reconstruction error. Left: learned de-anchored scores have nonzero negative mass or row-sum error before Markovization; after Markovization both diagnostics are exactly zero by construction. Middle: paired pre/post TV values show that Markovization is a validity restoration step rather than a TV-improvement heuristic. Right: the empirical repair ratio is close to one across environments and far below the deterministic bound $R_M \leq 2$.

Figure 2 shows nonzero negative mass and row error before post-processing, both exactly zero after Markovization. The repair ratio is well below 2 in all runs, with maximum about

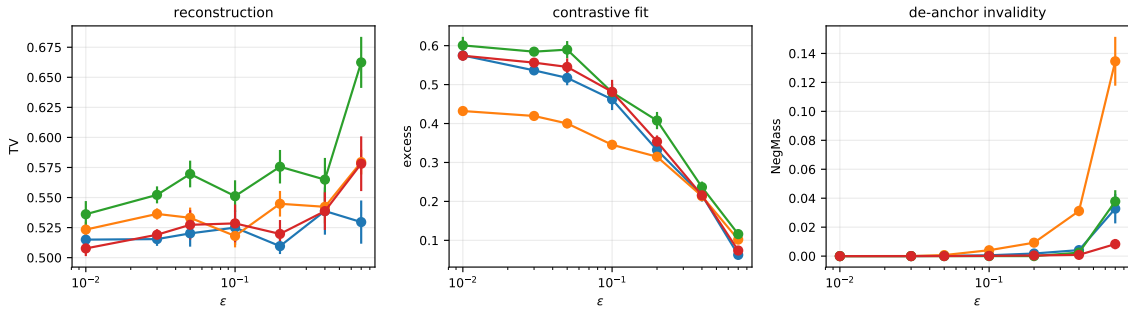


Figure 3: Anchor strength and reference-law coverage. Each ε and reference law is trained separately. Curves use the fixed reference-law order uniform, poor-coverage, empirical-KDE, and mixture in all three panels. The reconstruction TV has an interior optimum; poor reference coverage worsens reconstruction and invalidity.

1.03 and mean about 0.96. Thus Markovization is a validity-restoration step, not a TV-improvement heuristic.

8.4 Statistical rates, smoothness, and dimension

The third experiment is a real-trained one-dimensional rate diagnostic. We do not fill untrained high-dimensional settings with theory-shaped curves; each sample size and seed corresponds to a trained contrastive network, evaluated by $d_{\mu, \text{TV}}(\hat{K}_\theta, K_0)^2$.

The right panel of Figure 1 has the qualitative pattern predicted by the theory: increasing n reduces the reconstruction error. The fitted ordinary-least-squares log-log slopes for $d_{\mu, \text{TV}}(\hat{K}_\theta, K_0)^2$ are approximately 0.48 for the smooth model, 0.32 for the rough model, and 0.38 for the multimodal model. These slopes should not be read as precise estimates of the asymptotic exponent or as a high-dimensional benchmark; they are a sanity check that the real-trained reconstruction error decreases with sample size.

8.5 Anchor strength and reference-law coverage

The fourth experiment is a diagnostic for the two design parameters discussed in Section 3.3; it is not a claim that the paper solves optimal restart-law selection. We vary ε and the reference law, retraining a fresh network for each setting. The four reference curves use the fixed order uniform, poor-coverage, empirical-KDE, and mixture, with matched samplers and density evaluators. The experiment tests the conditioning–inversion tradeoff in ε and the effect of next-state reference coverage.

The observed TV curves show the expected conditioning–inversion tradeoff, with a problem-dependent best reference. High ε increases invalidity, especially for the poor-coverage reference, supporting the interpretation of ε as a genuine statistical parameter rather than a harmless technical constant.

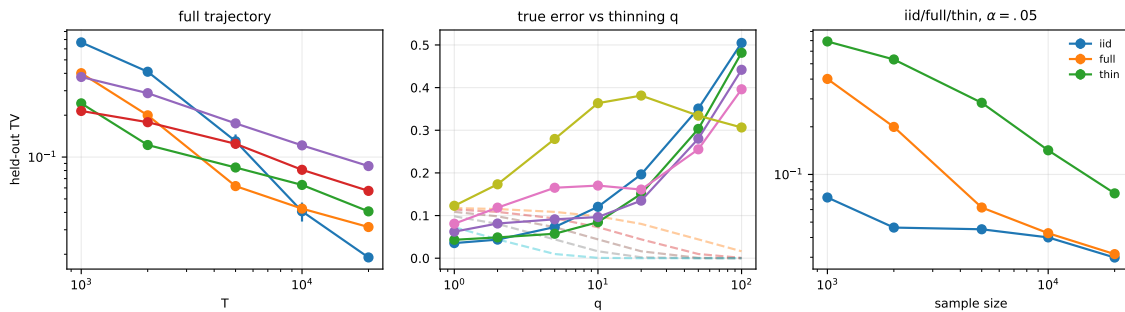


Figure 4: Trajectory-data stress test. Left: held-out TV decreases with trajectory length but worsens as mixing slows. Middle: thinning trades sample size for weaker dependence; colors use the same increasing- α order as the left panel. Right: i.i.d. transition pairs are easiest, full trajectories are harder, and thinning can help in the slow-mixing regime.

8.6 Trajectory-data stress test

The preceding oracle theory is stated for independent transition pairs. We therefore include a trajectory-only stress test on lazy finite-state chains, comparing adjacent transition-pair estimates with i.i.d. transition pairs and thinned trajectories. The experiment isolates temporal dependence; it is not used to claim sharp dependent-data rates or to analyze full-trajectory ERM. In the left and middle panels below, colors use increasing mixing parameter $\alpha \in \{0.02, 0.05, 0.1, 0.2, 0.5\}$.

Figure 4 shows the expected ordering: fast-mixing trajectories are closer to independent pairs, slow-mixing trajectories need larger T , and thinning can help in the slow-mixing regime. The result is consistent with the conservative thinning theorem in Section 6.2, but is not a sharp dependent-data rate claim.

8.7 Finite-horizon dynamical transfer and coverage failure

The sixth experiment closes the loop from learned one-step kernels to Markov dynamics. For each trained score we de-anchor, Markovize on a common grid, and roll out the resulting kernel. In the covered setting we take an initial law dominated by the design law and compute

$$\text{TV}(\xi \widehat{K}_\theta^m, \xi K_0^m), \quad m \in \{1, 2, 5, 10, 20, 50\}.$$

In the uncovered setting we use the rare-state construction $\mu(1) = \delta \in \{0.01, 0.02, 0.05\}$ and start from $\xi = \delta_1$. The displayed figure focuses on finite-horizon transfer and the coverage obstruction; stationary perturbation is already covered by Corollary 22.

In the covered setting, one-step integrated TV and rollout TV are strongly correlated (above 0.90 for every reported horizon and about 0.91 at horizon 10). The rare-state panel illustrates the obstruction behind Proposition 17: the design-averaged error is δ , but the one-step rollout error from the rare state is 1, an amplification factor $1/\delta$.

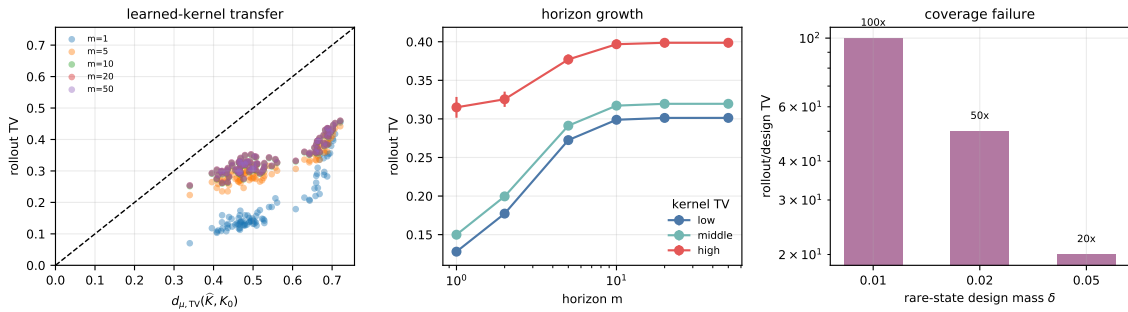


Figure 5: Dynamic transfer with learned kernels. Left: learned-kernel rollout errors across several horizons are controlled by one-step integrated TV. Middle: horizon growth is larger for learned kernels with larger one-step error. Right: without coverage, a small design-averaged error can be amplified by factors of 20–100 at one step.

Rare-state mass δ	$d_{\mu,TV}(K, L)$	rare-state rollout TV	amplification
0.01	0.01	1.00	100×
0.02	0.02	1.00	50×
0.05	0.05	1.00	20×

Table 2: Coverage-failure diagnostic. A design-averaged one-step error can be made small by assigning small design mass to a rare state, while rollout from that state remains maximally wrong. This table visualizes the obstruction in Proposition 17.

8.8 Ablation study

The seventh experiment removes one component at a time: anchoring, de-anchoring, Markovization, reference coverage, anchor strength, model capacity, and negative-sample count. The metrics are the same as above, so the ablation tests whether each interface component has an observable statistical or dynamical effect.

Table 3 compares the full valid-kernel pipeline with nearby interface variants and a row-normalized Gaussian-CDE baseline on the multimodal diagnostic. These comparisons are interface diagnostics, not benchmark claims: the full pipeline targets the original kernel, repairs validity after de-anchoring, and produces a kernel suitable for rollout.

The ablation confirms the intended division of labor. The invalidity columns are pre-Markovization diagnostics, so they do not contradict Theorem 9; no-deanchor is valid but targets $A_{\varepsilon,\nu}K_0$ rather than K_0 ; and no-Markov is not rolled out because it is not a valid kernel. The anchor is not presented as a universal finite-sample accuracy boost, but as the structural device that supplies the restart chart and lower envelope.

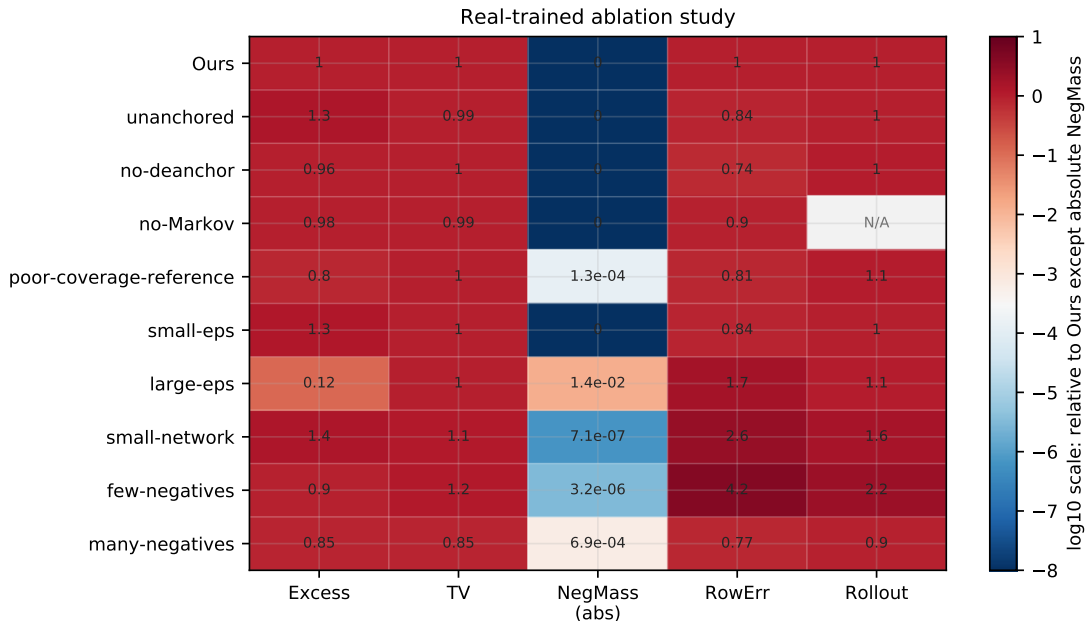


Figure 6: Ablation heatmap. Excess, TV, RowErr, and rollout entries are relative to Ours on a \log_{10} scale. The NegMass column instead reports absolute pre-Markovization negative mass, because Ours has zero NegMass to numerical precision; a 10^{-8} floor is used only for coloring zeros, not as a denominator. Removing anchoring, de-anchoring, Markovization, using an under-capacity network, or degrading reference coverage harms at least one of excess risk, TV reconstruction, invalidity, or rollout error.

Method	Role	Numerically valid?	Covered by chart theory?	$d_{\mu,TV}$	rollout TV
Ours	full interface	Yes	Yes	0.493	0.133
Ours-noMarkov	score without repair	No	No	0.489	N/A
Anchored-noDeanchor	wrong target kernel	Yes	No: targets $A_{\varepsilon,\nu}K_0$	0.495	0.14
Unanchored-NCE	accurate but no restart chart	Yes, after Markovization	No	0.489	0.136
Gaussian-CDE	row-normalized baseline	Yes	No	0.514	0.505

Table 3: Interface-oriented method comparison after end-to-end training. Numerical validity records whether the evaluated object is a transition kernel; theory coverage records whether the estimator is covered by the anchored-chart reconstruction theory. Gaussian-CDE is a row-normalized circular Gaussian regression baseline. No-Markov is not rolled out because it is not a valid transition kernel.

8.9 Runtime diagnostics

The final experiment gives measured runtime diagnostics for data construction, training, Markovization, and evaluation. No large-scale timing point is extrapolated.

Variant	Excess	TV	Pre-M NegMass	Pre-M RowErr	Num. valid?	Theory?	RolloutTV
Ours	0.427	0.493	0	0.13	Yes	Yes	0.133
unanchored	0.571	0.489	0	0.109	Yes	No	0.136
no-deanchor	0.411	0.495	N/A	N/A	Yes	No: wrong target	0.14
no-Markov	0.416	0.489	0	0.117	No	No	N/A
poor-coverage-reference	0.341	0.5	0.000134	0.105	Yes	stress test	0.149
small-eps	0.555	0.493	0	0.11	Yes	Yes	0.136
large-eps	0.0523	0.495	0.0138	0.226	Yes	Yes	0.145
small-network	0.599	0.556	7.14e-07	0.336	Yes	Yes	0.215
few-negatives	0.386	0.579	3.23e-06	0.542	Yes	Yes	0.299
many-negatives	0.364	0.419	0.000691	0.1	Yes	Yes	0.12

Table 4: Ablation summary from real-trained variants. Pre-M NegMass and Pre-M RowErr refer only to the de-anchored score before Markovization. N/A means that the corresponding pre-Markovization diagnostic or rollout is not defined for that ablation. Ours has zero Pre-M NegMass to numerical precision in this run. Numerical validity is separated from coverage by the anchored-chart theory. The no-Markov row is not rolled out because it is not a valid transition kernel.

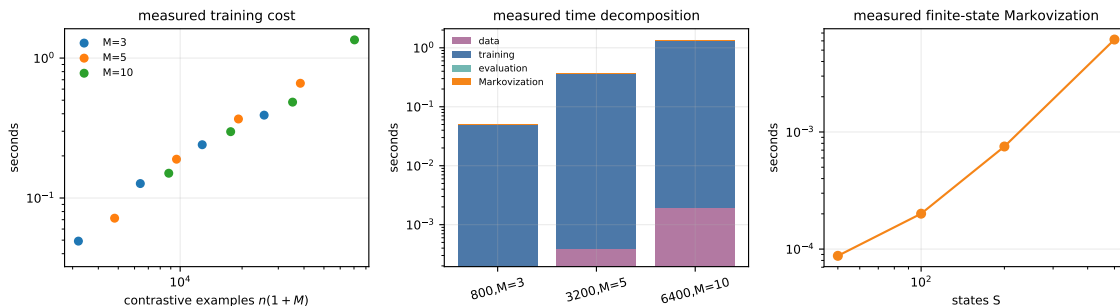


Figure 7: Runtime diagnostics. Left: measured training time versus the number of contrastive examples $n(1+M)$. Middle: representative measured wall-clock decomposition. Right: measured finite-state Markovization time.

Figure 7 shows the limited diagnostic we need: in these runs, the dominant cost is training the contrastive score network, while de-anchoring and Markovization are small post-processing costs. This is not a large-scale systems benchmark, and we do not make broader scalability claims.

9 Conclusion, Limitations, and Outlook

This paper introduced a Doeblin-anchored contrastive chart for learning Markov transition kernels. The chart organizes the learning problem through a sequence of quantitative

interfaces:

$$\begin{aligned} \text{contrastive risk} &\implies \text{anchored density} \\ &\implies \text{valid Markov kernel} \implies \text{finite-horizon dynamics.} \end{aligned}$$

Given a restart law and an anchor strength, the anchored transition is simultaneously a Doeblin-minorized Markov kernel, the positive conditional law in a binary contrastive experiment, and an explicitly invertible coordinate for the original transition law.

Within this chart, the anchored contrastive risk identifies the anchored transition density and calibrates excess risk to density error. De-anchoring recovers a score for the original transition law, while Markovization restores nonnegativity and row normalization with only a constant-factor loss in integrated L^1 accuracy. Standard oracle inequalities and Hölder–ReLU approximation bounds pass through the same interface. Under explicit occupancy coverage, valid-kernel error further controls finite-horizon marginal, path-law, and occupation-measure errors. For stationary geometrically β -mixing trajectories, a conservative thinning-and-coupling argument preserves the reconstruction interface with an effective sample size. The experiments serve as diagnostics of these interfaces rather than as leaderboard benchmarks.

The present analysis has several limitations. The main oracle theory is stated first for independent transition pairs, and the trajectory extension analyzes a thinned ERM rather than an estimator trained on every adjacent transition pair. The restart law must be simulable and sufficiently well supported; anchoring makes this role explicit but does not remove the reference-selection problem. The bounded-density assumptions provide uniform curvature and concentration, but exclude heavier-tailed settings. Finally, the main dynamical guarantee is finite-horizon and occupancy-weighted. It should not be read as a general stationary-distribution perturbation theorem.

Several extensions are natural. Sharper dependent-data analysis could treat full-trajectory ERM, nonstationary starts, and optimized mixing-rate dependence. Adaptive or data-dependent restart laws could improve statistical conditioning and, under restart-controlled data collection or additional design assumptions, downstream coverage. Tail-localized arguments could relax the global boundedness assumptions, while drift–minorization and nonuniform ergodicity techniques could extend the dynamical analysis beyond finite horizons. These directions can be pursued within the same contrastive-to-valid-kernel interface.

Acknowledgments and Disclosure of Funding

This work is supported by the Zhongguancun Academy, Grant No. C20250201.

Appendix A. Proofs and Technical Extensions

This appendix contains the proofs deferred from the main text and the auxiliary lemmas used in those proofs.

A.1 TV measurability

Lemma 18 (Measurability of the TV kernel error) *Let $(\mathcal{X}, \mathcal{B}_{\mathcal{X}})$ be a measurable space and $(\mathcal{Y}, \mathcal{B}_{\mathcal{Y}})$ be a standard Borel space. Let K, L be Markov kernels from \mathcal{X} to \mathcal{Y} . Then the map*

$$x \mapsto \text{TV}(K(x, \cdot), L(x, \cdot))$$

is measurable.

Proof On a standard Borel space, the σ -algebra $\mathcal{B}_{\mathcal{Y}}$ is countably generated. Let $\mathcal{C} \subset \mathcal{B}_{\mathcal{Y}}$ be a countable algebra generating $\mathcal{B}_{\mathcal{Y}}$. For any two probability measures P, Q on \mathcal{Y} , the finite measure $P + Q$ allows every $B \in \mathcal{B}_{\mathcal{Y}}$ to be approximated in $(P + Q)$ -measure by sets in \mathcal{C} . Hence

$$\text{TV}(K(x, \cdot), L(x, \cdot)) = \sup_{C \in \mathcal{C}} |K(x, C) - L(x, C)|,$$

which is a countable supremum of measurable functions of x and hence measurable. \blacksquare

A.2 Proof of Theorem 2

Part (i). Assume $0 < \varepsilon < 1$. If K is a Markov kernel, then for every x and B ,

$$A_{\varepsilon, \nu} K(x, B) = (1 - \varepsilon)K(x, B) + \varepsilon\nu(B) \geq \varepsilon\nu(B),$$

so $A_{\varepsilon, \nu} K$ lies in the stated image class. Conversely, if A is a Markov kernel with $A(x, B) \geq \varepsilon\nu(B)$, then $A(x, B) - \varepsilon\nu(B) \geq 0$ for all x and B . For each fixed x , define

$$K_x(B) := \frac{A(x, B) - \varepsilon\nu(B)}{1 - \varepsilon}.$$

Since $A(x, \cdot) - \varepsilon\nu(\cdot)$ is a nonnegative finite measure and

$$K_x(\mathbf{X}) = \frac{A(x, \mathbf{X}) - \varepsilon\nu(\mathbf{X})}{1 - \varepsilon} = 1,$$

K_x is a probability measure. Moreover, for each B , the map $x \mapsto K_x(B)$ is measurable, so K is a Markov kernel. The displayed inverse formula is verified by substituting:

$$A_{\varepsilon, \nu}^{-1}(A_{\varepsilon, \nu} K)(x, B) = \frac{(1 - \varepsilon)K(x, B) + \varepsilon\nu(B) - \varepsilon\nu(B)}{1 - \varepsilon} = K(x, B).$$

Part (ii). For every design law μ ,

$$\begin{aligned} d_{\mu, \text{TV}}(A_{\varepsilon, \nu} K, A_{\varepsilon, \nu} L) &= \int \text{TV}(A_{\varepsilon, \nu} K(x, \cdot), A_{\varepsilon, \nu} L(x, \cdot)) \mu(\mathrm{d}x) \\ &= \int \text{TV}((1 - \varepsilon)K(x, \cdot) + \varepsilon\nu, (1 - \varepsilon)L(x, \cdot) + \varepsilon\nu) \mu(\mathrm{d}x). \end{aligned}$$

Since the signed difference satisfies

$$((1 - \varepsilon)K(x, \cdot) + \varepsilon\nu) - ((1 - \varepsilon)L(x, \cdot) + \varepsilon\nu) = (1 - \varepsilon)(K(x, \cdot) - L(x, \cdot)),$$

the total variation norm is positively homogeneous, and hence

$$\text{TV}((1 - \varepsilon)K(x, \cdot) + \varepsilon\nu, (1 - \varepsilon)L(x, \cdot) + \varepsilon\nu) = (1 - \varepsilon)\text{TV}(K(x, \cdot), L(x, \cdot)).$$

Integrating gives $d_{\mu, \text{TV}}(A_{\varepsilon, \nu}K, A_{\varepsilon, \nu}L) = (1 - \varepsilon)d_{\mu, \text{TV}}(K, L)$. The uniform version is analogous.

Part (iii). If $r(y) > 0$ and $a(y | x) > 0$, then $\eta_{A, a}(x, y) = a(y | x) / \{a(y | x) + \tau r(y)\}$ is well-defined and satisfies $0 < \eta_{A, a} < 1$. Solving for a gives $a = \tau r \eta / (1 - \eta)$. Substituting into the inverse anchor map and simplifying gives the de-anchoring formula. The almost-everywhere qualifier follows because all identities hold for $\mu \otimes \lambda$ -almost every (x, y) when $r > 0$ λ -a.e.

A.3 Proof of Theorem 6

Part (i): Identification. Fix (x, y) and abbreviate $p = a_0(y | x)$, $q = \tau r(y)$, $s = a(y | x)$. The pointwise integrand of (2), up to an s -independent term, equals

$$F_{p, q}(s) := -p \log s + (p + q) \log(s + q).$$

One checks that

$$F'_{p, q}(s) = -\frac{p}{s} + \frac{p + q}{s + q} = \frac{q(s - p)}{s(s + q)}.$$

Hence $s = p$ is the unique minimizer. Since $F_{p, q}(s) - F_{p, q}(p) \geq 0$ pointwise and equality holds if and only if $s = p$, integration implies that the population risk is uniquely minimized by $a = a_0$, up to $\mu \otimes \lambda$ -a.e. equality.

Part (ii): L^2 calibration. By Assumption 4, $a_0 = (1 - \varepsilon)k_0 + \varepsilon r$ satisfies $\varepsilon r_- \leq a_0(y | x) \leq (1 - \varepsilon)M_0 + \varepsilon r_+$. By Assumption 5, every $a \in \mathcal{A}_n$ lies in $[\gamma, \Gamma]$. Hence the triples (p, q, s) with $p = a_0(y | x)$, $q = \tau r(y)$, and $s = a(y | x)$ lie in a compact subset of $(0, \infty)^3$ bounded away from zero. Define

$$G(p, q, s) := \begin{cases} \frac{F_{p, q}(s) - F_{p, q}(p)}{(s - p)^2}, & s \neq p, \\ \frac{1}{2} F''_{p, q}(p), & s = p. \end{cases}$$

Since $s = p$ is the unique minimizer of $F_{p, q}$, the numerator is strictly positive whenever $s \neq p$. The above definition extends continuously to $s = p$, and $F''_{p, q}(p) > 0$ on the admissible compact set. Hence G is continuous and strictly positive on the compact admissible set. Therefore there exist constants $0 < c_- \leq c_+ < \infty$, depending only on the boundedness constants, such that

$$c_-(s - p)^2 \leq F_{p, q}(s) - F_{p, q}(p) \leq c_+(s - p)^2.$$

Integrating gives the $L^2(\mu \otimes \lambda)$ calibration.

Part (iii): Contrastive KL representation. A direct algebraic computation shows

$$\begin{aligned}
 & F_{p,q}(s) - F_{p,q}(p) \\
 &= p \log \frac{p}{s} + (p+q) \log \frac{s+q}{p+q} \\
 &= p \log \frac{p/(p+q)}{s/(s+q)} + q \log \frac{q/(p+q)}{q/(s+q)} \\
 &= (p+q) \text{KL} \left(\text{Ber} \left(\frac{p}{p+q} \right) \parallel \text{Ber} \left(\frac{s}{s+q} \right) \right),
 \end{aligned}$$

which is the integrand in (4) after substituting $p = a_0$, $q = \tau r$, $s = a$.

Part (iv): L^1 and Hellinger consequences. Assuming $\lambda(\mathcal{Y}) = 1$, the product measure $\mu \otimes \lambda$ is a probability measure. By Cauchy–Schwarz on $\mu \otimes \lambda$,

$$\|a - a_0\|_{1,\mu\lambda}^2 \leq \|a - a_0\|_{2,\mu\lambda}^2 \leq c_-^{-1} \mathcal{E}(a).$$

For Hellinger, since $a_0 \geq \varepsilon r_-$ and $a \geq \gamma$, both functions are bounded below by $m_a = \min\{\varepsilon r_-, \gamma\} > 0$. The pointwise bound

$$(\sqrt{a} - \sqrt{a_0})^2 = \frac{(a - a_0)^2}{(\sqrt{a} + \sqrt{a_0})^2} \leq \frac{(a - a_0)^2}{4m_a}$$

integrates to the Hellinger calibration. If a is itself a transition density and $A_a(x, dy) = a(y | x)\lambda(dy)$, then

$$d_{\mu,\text{TV}}(A_a, A_{\varepsilon,\nu}K_0) = \frac{1}{2} \|a - a_0\|_{1,\mu\lambda}.$$

Therefore

$$d_{\mu,\text{TV}}(A_a, A_{\varepsilon,\nu}K_0)^2 \leq \frac{1}{4} \|a - a_0\|_{1,\mu\lambda}^2 \leq \frac{1}{4c_-} \mathcal{E}(a).$$

A.4 Proof of Theorem 7

Before presenting the complete proof of Theorem 7, we first introduce the following two lemmas.

Lemma 19 *Under Assumptions 4 and 5, there is a constant $L_\ell < \infty$, depending only on $(\tau, r_-, r_+, \gamma, \Gamma)$, such that for all $a, \bar{a} \in \mathcal{A}_n$ with $\|a - \bar{a}\|_\infty \leq \delta$,*

$$|\mathcal{R}(a) - \mathcal{R}(\bar{a})| \leq L_\ell \delta, \quad \left| \widehat{\mathcal{R}}_n(a) - \widehat{\mathcal{R}}_n(\bar{a}) \right| \leq L_\ell \delta.$$

Proof Recall that for any candidate $a \in \mathcal{A}_n$ and fixed (x, y) , the positive and negative loss components are

$$\ell_a^+(x, y) = -\log \frac{a(y | x)}{a(y | x) + \tau r(y)}, \quad \ell_a^-(x, y) = -\log \frac{\tau r(y)}{a(y | x) + \tau r(y)}.$$

For a fixed (x, y) , let $s = a(y | x)$ and $q = \tau r(y)$. Under Assumptions 4 and 5, we have $s \in [\gamma, \Gamma]$ and $q \in [\tau r_-, \tau r_+]$. Viewed as functions of s , the loss components are $f^+(s) := -\log(s) + \log(s+q)$ and $f^-(s) := -\log(q) + \log(s+q)$.

Their derivatives with respect to s are given by

$$\left| \frac{d}{ds} f^+(s) \right| = \left| -\frac{1}{s} + \frac{1}{s+q} \right| = \frac{q}{s(s+q)}, \quad \left| \frac{d}{ds} f^-(s) \right| = \frac{1}{s+q}.$$

We can uniformly bound these derivatives on the admissible domain $[\gamma, \Gamma] \times [\tau r_-, \tau r_+]$:

$$\left| \frac{d}{ds} f^+(s) \right| \leq \frac{\tau r_+}{\gamma(\gamma + \tau r_-)} =: L^+, \quad \left| \frac{d}{ds} f^-(s) \right| \leq \frac{1}{\gamma + \tau r_-} =: L^-.$$

By the Mean Value Theorem, the loss functions are Lipschitz continuous in the candidate score $a(y | x)$. For any $a, \bar{a} \in \mathcal{A}_n$ with $\|a - \bar{a}\|_\infty \leq \delta$, it follows pointwise that

$$|\ell_a^+(x, y) - \ell_{\bar{a}}^+(x, y)| \leq L^+ \delta, \quad |\ell_a^-(x, y) - \ell_{\bar{a}}^-(x, y)| \leq L^- \delta.$$

The empirical risk $\widehat{\mathcal{R}}_n$ is a linear combination of these loss terms. By the triangle inequality, for any realization of the augmented dataset,

$$\begin{aligned} \left| \widehat{\mathcal{R}}_n(a) - \widehat{\mathcal{R}}_n(\bar{a}) \right| &\leq \frac{1}{n} \sum_{i=1}^n \left[(1 - \varepsilon) \left| \ell_a^+(X_i, Y_i) - \ell_{\bar{a}}^+(X_i, Y_i) \right| \right. \\ &\quad \left. + \varepsilon \left| \ell_a^+(X_i, \tilde{Y}_i) - \ell_{\bar{a}}^+(X_i, \tilde{Y}_i) \right| + \sum_{j=1}^{\tau} \left| \ell_a^-(X_i, Z_{ij}) - \ell_{\bar{a}}^-(X_i, Z_{ij}) \right| \right] \\ &\leq (1 - \varepsilon) L^+ \delta + \varepsilon L^+ \delta + \tau L^- \delta \\ &= (L^+ + \tau L^-) \delta. \end{aligned}$$

Setting $L_\ell := L^+ + \tau L^-$ yields the uniform bound for the empirical risk. Since this pointwise bound holds surely, integrating with respect to the population distribution immediately yields the identical bound $|\mathcal{R}(a) - \mathcal{R}(\bar{a})| \leq L_\ell \delta$ for the population risk. \blacksquare

Lemma 20 (Entropy bound on the uniform deviation) *Under Assumptions 4 and 5, there exists a constant $B_\ell < \infty$, depending only on $(\tau, r_-, r_+, \gamma, \Gamma)$, such that, with*

$$\Delta_n := \mathbb{E} \sup_{a \in \mathcal{A}_n} \left| \widehat{\mathcal{R}}_n(a) - \mathcal{R}(a) \right|,$$

for every $\delta > 0$,

$$\Delta_n \leq 2L_\ell \delta + B_\ell \sqrt{\frac{2 \log(2N_\infty^{\text{int}}(\delta, \mathcal{A}_n))}{n}}.$$

Proof Since $a \in [\gamma, \Gamma]$ and $r \in [r_-, r_+]$, both ℓ_a^+ and ℓ_a^- are uniformly bounded. Moreover, the one-block loss $g_a(B)$ is a fixed finite linear combination of these bounded terms, so there exists a constant $B_\ell < \infty$ such that $|g_a(B)| \leq B_\ell$ uniformly over $a \in \mathcal{A}_n$.

Let $\{a_1, \dots, a_N\}$ be a δ -cover of \mathcal{A}_n in the sup-norm, where $N = N_\infty^{\text{int}}(\delta, \mathcal{A}_n)$. For any arbitrary $a \in \mathcal{A}_n$, we can select a cover point a_j such that $\|a - a_j\|_\infty \leq \delta$. By the bounded loss and Lipschitz covering reduction (Lemma 19), we have both

$$\left| \widehat{\mathcal{R}}_n(a) - \widehat{\mathcal{R}}_n(a_j) \right| \leq L_\ell \delta \quad \text{and} \quad |\mathcal{R}(a) - \mathcal{R}(a_j)| \leq L_\ell \delta.$$

Applying the triangle inequality, the uniform deviation can be bounded by the maximum deviation over the finite cover:

$$\begin{aligned} \sup_{a \in \mathcal{A}_n} \left| \widehat{\mathcal{R}}_n(a) - \mathcal{R}(a) \right| &\leq \sup_{a \in \mathcal{A}_n} \left(\left| \widehat{\mathcal{R}}_n(a) - \widehat{\mathcal{R}}_n(a_j) \right| + \left| \widehat{\mathcal{R}}_n(a_j) - \mathcal{R}(a_j) \right| + \left| \mathcal{R}(a_j) - \mathcal{R}(a) \right| \right) \\ &\leq \max_{j=1, \dots, N} \left| \widehat{\mathcal{R}}_n(a_j) - \mathcal{R}(a_j) \right| + 2L_\ell \delta. \end{aligned}$$

Taking expectations on both sides, it remains to bound the expected maximum of the empirical processes. Since $|g_{a_j}(B)| \leq B_\ell$, the centered variables $g_{a_j}(B) - \mathbb{E}g_{a_j}(B)$ are uniformly bounded by $2B_\ell$. Enlarging B_ℓ if necessary, Hoeffding's lemma implies that $\widehat{\mathcal{R}}_n(a_j) - \mathcal{R}(a_j)$ is sub-Gaussian with variance proxy of order B_ℓ^2/n . Since $|Z| = \max\{Z, -Z\}$, the maximum of the absolute values corresponds to the maximum of $2N$ sub-Gaussian random variables. By the standard maximal inequality for finite sub-Gaussian classes (e.g., Massart's lemma (Boucheron et al., 2013)), we obtain

$$\mathbb{E} \left[\max_{j=1, \dots, N} \left| \widehat{\mathcal{R}}_n(a_j) - \mathcal{R}(a_j) \right| \right] \leq B_\ell \sqrt{\frac{2 \log(2N)}{n}}.$$

Adding the $2L_\ell \delta$ deterministic approximation error yields the stated entropy bound. \blacksquare

We now present the complete proof of Theorem 7.

Part (i). Fix any $a^* \in \mathcal{A}_n$. Since \widehat{a}_n is δ_{opt} -optimal for the empirical risk,

$$\widehat{\mathcal{R}}_n(\widehat{a}_n) \leq \widehat{\mathcal{R}}_n(a^*) + \delta_{\text{opt}}.$$

Add and subtract population risks to obtain

$$\begin{aligned} \mathcal{R}(\widehat{a}_n) - \mathcal{R}(a_0) &\leq \left[\mathcal{R}(\widehat{a}_n) - \widehat{\mathcal{R}}_n(\widehat{a}_n) \right] + \delta_{\text{opt}} + \left[\widehat{\mathcal{R}}_n(a^*) - \mathcal{R}(a^*) \right] + [\mathcal{R}(a^*) - \mathcal{R}(a_0)] \\ &\leq 2 \sup_{a \in \mathcal{A}_n} \left| \widehat{\mathcal{R}}_n(a) - \mathcal{R}(a) \right| + \delta_{\text{opt}} + [\mathcal{R}(a^*) - \mathcal{R}(a_0)]. \end{aligned}$$

Theorem 6(ii) and the upper calibration bound give

$$\left\| \widetilde{k}_{\widehat{a}_n} - k_0 \right\|_{2, \mu_\lambda}^2 \leq \frac{2}{(1-\varepsilon)^2 c_-} \sup_{a \in \mathcal{A}_n} \left| \widehat{\mathcal{R}}_n(a) - \mathcal{R}(a) \right| + \frac{\delta_{\text{opt}}}{(1-\varepsilon)^2 c_-} + \frac{c_+}{(1-\varepsilon)^2 c_-} \|a^* - a_0\|_{2, \mu_\lambda}^2.$$

Taking expectations on both sides and taking the infimum over $a^* \in \mathcal{A}_n$, we obtain, by the definition of the expected uniform deviation

$$\Delta_n := \mathbb{E} \sup_{a \in \mathcal{A}_n} \left| \widehat{\mathcal{R}}_n(a) - \mathcal{R}(a) \right|,$$

the following intermediate bound:

$$\mathbb{E} \left\| \widetilde{k}_{\widehat{a}_n} - k_0 \right\|_{2, \mu_\lambda}^2 \leq \frac{2\Delta_n + \delta_{\text{opt}}}{(1-\varepsilon)^2 c_-} + \frac{c_+}{(1-\varepsilon)^2 c_-} \inf_{a \in \mathcal{A}_n} \|a - a_0\|_{2, \mu_\lambda}^2.$$

Finally, applying Lemma 20 to upper-bound Δ_n yields the stated entropy bound.

Part (ii). The blocks are i.i.d. by construction. By Assumption 4, a_0 is bounded above and below by positive constants, and by Assumption 5, every $a \in \mathcal{A}_n$ lies in $[\gamma, \Gamma]$, while

$$\varepsilon r_- \leq a_0(y | x) \leq (1 - \varepsilon)M_0 + \varepsilon r_+$$

almost everywhere. Hence both a and a_0 take values in the common compact interval

$$[m, M], \quad m := \min\{\gamma, \varepsilon r_-\}, \quad M := \max\{\Gamma, (1 - \varepsilon)M_0 + \varepsilon r_+\}.$$

On this interval the two scalar loss maps are uniformly Lipschitz. Therefore, the maps

$$s \mapsto -\log \frac{s}{s + \tau r(y)}, \quad s \mapsto -\log \frac{\tau r(y)}{s + \tau r(y)}$$

are uniformly Lipschitz in s over the admissible range, with a Lipschitz constant depending only on $(\varepsilon, \tau, r_-, r_+, M_0, \gamma, \Gamma)$. Hence,

$$|\ell_a^\pm(X, U) - \ell_{a_0}^\pm(X, U)| \leq L |a(U | X) - a_0(U | X)| \text{ a.s.}$$

Therefore

$$\begin{aligned} |g_a(B) - g_{a_0}(B)| &\leq L \left((1 - \varepsilon) |a(Y | X) - a_0(Y | X)| + \varepsilon |a(\tilde{Y} | X) - a_0(\tilde{Y} | X)| \right) \\ &\quad + L \left(\sum_{j=1}^{\tau} |a(Z_j | X) - a_0(Z_j | X)| \right). \end{aligned}$$

Since all terms are uniformly bounded, this also gives the almost-sure bound

$$|g_a(B) - g_{a_0}(B)| \leq B_h.$$

For the second moment, use $(u_1 + \dots + u_m)^2 \leq m \sum_i u_i^2$. Conditional on $X = x$, the Y -term is integrated against $K_0(x, dy) = k_0(y | x)\lambda(dy)$, and the reference terms are integrated against $\nu(dy) = r(y)\lambda(dy)$. Since $k_0 \leq M_0$ and $r \leq r_+$, all these integrals are bounded by a constant times

$$\int |a(y | x) - a_0(y | x)|^2 \lambda(dy).$$

Integrating over $x \sim \mu$ yields

$$\mathbb{E}[(g_a(B) - g_{a_0}(B))^2] \leq C \|a - a_0\|_{2, \mu\lambda}^2.$$

By the lower calibration inequality in Theorem 6,

$$\|a - a_0\|_{2, \mu\lambda}^2 \leq c^{-1} \mathcal{E}(a),$$

and hence

$$\mathbb{E}[(g_a(B) - g_{a_0}(B))^2] \leq V_\ell \mathcal{E}(a).$$

Part (iii). Let $h_a := g_a - g_{a_0}$. Then $\mathbb{E}h_a = \mathcal{E}(a)$. By part (ii), every centered variable $h_a(B) - \mathbb{E}h_a(B)$ is bounded in absolute value by $2B_h$ and has variance at most $V_\ell \mathcal{E}(a)$. The

standard bounded Bernstein inequality (Boucheron et al., 2013; Vershynin, 2018) gives, for fixed a and $t > 0$,

$$\mathbb{P}\left(\left|(\widehat{\mathcal{R}}_n - \mathcal{R})(a) - (\widehat{\mathcal{R}}_n - \mathcal{R})(a_0)\right| > \sqrt{\frac{2V_\ell \mathcal{E}(a)t}{n}} + \frac{4B_h t}{3n}\right) \leq 2e^{-t}.$$

The inequality $\sqrt{xy} \leq x/8 + 2y$ for $x, y \geq 0$ implies that the deviation on the left is at most

$$\frac{1}{4}\mathcal{E}(a) + C_0 \frac{t}{n}$$

outside the same exceptional event, for a constant C_0 depending only on V_ℓ and B_h .

Let $a_1, \dots, a_N \in \mathcal{A}_n$ be an internal sup-norm δ -cover of \mathcal{A}_n , where

$$N = N_\infty^{\text{int}}(\delta, \mathcal{A}_n).$$

Set

$$u := \log \frac{2N}{\eta}.$$

Applying the preceding bound with $t = u$ and taking a union bound over the cover, we obtain an event \mathcal{E} with $\mathbb{P}(\mathcal{E}) \geq 1 - \eta$ such that, on \mathcal{E} , simultaneously for $j = 1, \dots, N$,

$$\left|(\widehat{\mathcal{R}}_n - \mathcal{R})(a_j) - (\widehat{\mathcal{R}}_n - \mathcal{R})(a_0)\right| \leq \frac{1}{4}\mathcal{E}(a_j) + C_0 \frac{u}{n}. \quad (10)$$

Work on the event \mathcal{E} . For any $a \in \mathcal{A}_n$, choose a cover point $\bar{a} \in \{a_1, \dots, a_N\}$ such that

$$\|a - \bar{a}\|_\infty \leq \delta.$$

By Lemma 19,

$$|\mathcal{R}(a) - \mathcal{R}(\bar{a})| \leq L_\ell \delta, \quad \left|\widehat{\mathcal{R}}_n(a) - \widehat{\mathcal{R}}_n(\bar{a})\right| \leq L_\ell \delta. \quad (11)$$

Let \bar{a}_n be a cover point of \widehat{a}_n , and fix an arbitrary comparator $a^* \in \mathcal{A}_n$ with cover point \bar{a}^* . By (11) and the δ_{opt} -optimality of \widehat{a}_n ,

$$\begin{aligned} \widehat{\mathcal{R}}_n(\bar{a}_n) &\leq \widehat{\mathcal{R}}_n(\widehat{a}_n) + L_\ell \delta \\ &\leq \widehat{\mathcal{R}}_n(a^*) + L_\ell \delta + \delta_{\text{opt}} \\ &\leq \widehat{\mathcal{R}}_n(\bar{a}^*) + 2L_\ell \delta + \delta_{\text{opt}}. \end{aligned} \quad (12)$$

We now compare the excess risks on the net. Applying (10) to \bar{a}_n gives

$$\begin{aligned} \mathcal{E}(\bar{a}_n) &= \mathcal{R}(\bar{a}_n) - \mathcal{R}(a_0) \\ &\leq \widehat{\mathcal{R}}_n(\bar{a}_n) - \widehat{\mathcal{R}}_n(a_0) + \frac{1}{4}\mathcal{E}(\bar{a}_n) + C_0 \frac{u}{n}. \end{aligned} \quad (13)$$

Combining (13) with (12), we obtain

$$\mathcal{E}(\bar{a}_n) \leq \widehat{\mathcal{R}}_n(\bar{a}^*) - \widehat{\mathcal{R}}_n(a_0) + 2L_\ell \delta + \delta_{\text{opt}} + \frac{1}{4}\mathcal{E}(\bar{a}_n) + C_0 \frac{u}{n}. \quad (14)$$

Applying (10) to \bar{a}^* gives

$$\widehat{\mathcal{R}}_n(\bar{a}^*) - \widehat{\mathcal{R}}_n(a_0) \leq \mathcal{E}(\bar{a}^*) + \frac{1}{4}\mathcal{E}(\bar{a}^*) + C_0\frac{u}{n}. \quad (15)$$

Substituting (15) into (14) yields

$$\mathcal{E}(\bar{a}_n) \leq \frac{5}{4}\mathcal{E}(\bar{a}^*) + 2L_\ell\delta + \delta_{\text{opt}} + \frac{1}{4}\mathcal{E}(\bar{a}_n) + 2C_0\frac{u}{n}. \quad (16)$$

Rearranging gives

$$\mathcal{E}(\bar{a}_n) \leq \frac{5}{3}\mathcal{E}(\bar{a}^*) + \frac{8}{3}L_\ell\delta + \frac{4}{3}\delta_{\text{opt}} + \frac{8}{3}C_0\frac{u}{n}. \quad (17)$$

By (11),

$$\mathcal{E}(\widehat{a}_n) \leq \mathcal{E}(\bar{a}_n) + L_\ell\delta, \quad \mathcal{E}(\bar{a}^*) \leq \mathcal{E}(a^*) + L_\ell\delta. \quad (18)$$

Combining (17) and (18), we obtain

$$\mathcal{E}(\widehat{a}_n) \leq \frac{5}{3}\mathcal{E}(a^*) + \frac{16}{3}L_\ell\delta + \frac{4}{3}\delta_{\text{opt}} + \frac{8}{3}C_0\frac{u}{n}.$$

Since $a^* \in \mathcal{A}_n$ was arbitrary, taking the infimum over $a^* \in \mathcal{A}_n$ and using $u = \log(2N/\eta)$ gives

$$\mathcal{E}(\widehat{a}_n) \leq \frac{5}{3} \inf_{a \in \mathcal{A}_n} \mathcal{E}(a) + C_{\text{fast}} \left[L_\ell\delta + \delta_{\text{opt}} + \frac{\log\{2N_\infty^{\text{int}}(\delta, \mathcal{A}_n)/\eta\}}{n} \right],$$

with probability at least $1 - \eta$. Enlarging C_{fast} if necessary, this can be written as

$$\mathcal{E}(\widehat{a}_n) \leq C_{\text{fast}} \left[\inf_{a \in \mathcal{A}_n} \mathcal{E}(a) + L_\ell\delta + \delta_{\text{opt}} + \frac{\log\{2N_\infty^{\text{int}}(\delta, \mathcal{A}_n)/\eta\}}{n} \right]. \quad (19)$$

By Theorem 6(ii), on the same event,

$$\left\| \widetilde{k}_{\widehat{a}_n} - k_0 \right\|_{2,\mu\lambda}^2 \leq \frac{1}{(1-\varepsilon)^2 c_-} \mathcal{E}(\widehat{a}_n).$$

Combining this inequality with (19) yields

$$\left\| \widetilde{k}_{\widehat{a}_n} - k_0 \right\|_{2,\mu\lambda}^2 \leq \frac{C_{\text{fast}}}{(1-\varepsilon)^2 c_-} \left[\inf_{a \in \mathcal{A}_n} \mathcal{E}(a) + L_\ell\delta + \delta_{\text{opt}} + \frac{\log\{2N_\infty^{\text{int}}(\delta, \mathcal{A}_n)/\eta\}}{n} \right].$$

All numerical constants are absorbed into C_{fast} , which depends only on the boundedness constants and on τ .

A.5 Proof of Theorem 9

Define

$$c_g(x) := \int g^+(y | x) \lambda(dy).$$

By the assumed $L^1(\lambda)$ -integrability of $g(\cdot | x)$, we have $0 \leq c_g(x) < \infty$ for every x . Joint measurability of $\mathfrak{M}g$ follows because g^+ is jointly measurable and $x \mapsto c_g(x)$ is measurable;

the ratio $g^+(y | x)/c_g(x)$ is measurable on the set $\{x : c_g(x) > 0\}$, and the fallback $r(y)$ is jointly measurable. In either case, $\mathfrak{M}g(\cdot | x) \geq 0$ and

$$\int \mathfrak{M}g(y | x) \lambda(dy) = 1.$$

Thus $\mathfrak{M}g$ is a transition density.

For the L^1 bound, fix x . If $c_g(x) = 0$, then $g^+ = 0$ λ -a.e., hence $g \leq 0$ λ -a.e. Since k is a transition density,

$$\int |g - k| d\lambda \geq \int k d\lambda = 1.$$

On the other hand, $\mathfrak{M}g = r$ is a probability density, and therefore

$$\int |\mathfrak{M}g - k| d\lambda \leq \int \mathfrak{M}g d\lambda + \int k d\lambda = 2 \leq 2 \int |g - k| d\lambda.$$

Now suppose $c_g(x) > 0$. Write

$$\delta := \int |g - k| d\lambda, \quad \delta_+ := \int |g^+ - k| d\lambda.$$

Since $k \geq 0$, replacing g by g^+ cannot increase the distance to k . Hence

$$\delta_+ \leq \delta.$$

Then

$$\begin{aligned} \int \left| \frac{g^+}{c_g} - k \right| d\lambda &\leq \int \left| \frac{g^+}{c_g} - g^+ \right| d\lambda + \int |g^+ - k| d\lambda \\ &= |1 - c_g| + \delta_+. \end{aligned}$$

Moreover,

$$|1 - c_g| = \left| \int k d\lambda - \int g^+ d\lambda \right| \leq \int |k - g^+| d\lambda = \delta_+.$$

Therefore

$$\int |\mathfrak{M}g - k| d\lambda \leq 2\delta_+ \leq 2\delta.$$

This proves the pointwise L^1 bound. Integrating with respect to μ gives

$$\|\mathfrak{M}g - k\|_{1,\mu\lambda} \leq 2\|g - k\|_{1,\mu\lambda}.$$

Taking $g = \tilde{k}_{\hat{a}_n}$ and $k = k_0$, we get

$$\|\hat{k}_n - k_0\|_{1,\mu\lambda} \leq 2\|\tilde{k}_{\hat{a}_n} - k_0\|_{1,\mu\lambda}.$$

Since total variation is one half of the L^1 distance between densities,

$$d_{\mu,\text{TV}}(\hat{K}_n, K_0) \leq \|\tilde{k}_{\hat{a}_n} - k_0\|_{1,\mu\lambda}.$$

By Cauchy–Schwarz,

$$d_{\mu,\text{TV}}(\hat{K}_n, K_0)^2 \leq \|\tilde{k}_{\hat{a}_n} - k_0\|_{2,\mu\lambda}^2.$$

The bound (8) follows from Theorem 7(iii).

A.6 Proof of Theorem 11

Set $\bar{d} := 2d$. We first prove the high-probability upper bound.

Let

$$S_n := \left\lceil n^{\bar{d}/(2\beta+\bar{d})} \right\rceil, \quad \mathcal{A}_n := \mathcal{A}(S_n).$$

By Assumption 10, the class \mathcal{A}_n consists of jointly measurable functions taking values in $[\gamma, \Gamma]$, so Assumption 5 holds for \mathcal{A}_n . The same assumption also gives an approximant $a_n^\circ \in \mathcal{A}_n$ satisfying

$$\|a_n^\circ - a_0\|_\infty \leq C_{\text{app}} S_n^{-\beta/\bar{d}} (\log S_n)^{\kappa_{\text{app}}}.$$

Since $\mu \otimes \lambda$ is a probability measure, this implies

$$\|a_n^\circ - a_0\|_{2,\mu\lambda}^2 \leq C_{\text{app}}^2 S_n^{-2\beta/\bar{d}} (\log S_n)^{2\kappa_{\text{app}}}.$$

By the upper calibration bound in Theorem 6(ii),

$$\inf_{a \in \mathcal{A}_n} \mathcal{E}(a) \leq c_+ \inf_{a \in \mathcal{A}_n} \|a - a_0\|_{2,\mu\lambda}^2 \leq C S_n^{-2\beta/\bar{d}} (\log S_n)^{2\kappa_{\text{app}}}.$$

Here and below $C < \infty$ denotes a generic constant independent of n and η .

Apply Theorem 7(iii) with covering radius $\delta = n^{-1}$. With probability at least $1 - \eta$,

$$\mathcal{E}(\hat{a}_n) \leq C_{\text{fast}} \left[\inf_{a \in \mathcal{A}_n} \mathcal{E}(a) + L_\ell n^{-1} + \delta_{\text{opt}} + \frac{\log\{2N_\infty^{\text{int}}(n^{-1}, \mathcal{A}_n)/\eta\}}{n} \right].$$

By Assumption 10,

$$\log N_\infty^{\text{int}}(n^{-1}, \mathcal{A}_n) \leq C_{\text{ent}} S_n (\log n)^{\kappa_{\text{ent}}}, \quad n \geq 3.$$

Therefore, on the same event,

$$\mathcal{E}(\hat{a}_n) \leq C \left[S_n^{-2\beta/\bar{d}} (\log S_n)^{2\kappa_{\text{app}}} + \frac{1}{n} + \delta_{\text{opt}} + \frac{S_n (\log n)^{\kappa_{\text{ent}}}}{n} + \frac{\log(1/\eta)}{n} \right].$$

The choice of S_n gives

$$S_n^{-2\beta/\bar{d}} \leq C n^{-2\beta/(2\beta+\bar{d})}, \quad \frac{S_n}{n} \leq C n^{-2\beta/(2\beta+\bar{d})}.$$

Since $2\beta/(2\beta+\bar{d}) < 1$, the term n^{-1} is also bounded by a constant multiple of $n^{-2\beta/(2\beta+\bar{d})}$ for $n \geq 3$. Absorbing all logarithmic powers into a single exponent $\kappa < \infty$, we obtain

$$\mathcal{E}(\hat{a}_n) \leq C \left[n^{-2\beta/(2\beta+\bar{d})} (\log n)^\kappa + \delta_{\text{opt}} + \frac{\log(1/\eta)}{n} \right].$$

By Theorem 6(ii),

$$\left\| \tilde{k}_n - k_0 \right\|_{2,\mu\lambda}^2 \leq \frac{1}{(1-\varepsilon)^2 c_-} \mathcal{E}(\hat{a}_n).$$

Thus, enlarging C if necessary,

$$\left\| \tilde{k}_n - k_0 \right\|_{2,\mu\lambda}^2 \leq C \left[n^{-2\beta/(2\beta+\bar{d})} (\log n)^\kappa + \delta_{\text{opt}} + \frac{\log(1/\eta)}{n} \right].$$

For the Markovized estimator, we use Theorem 9 directly. Applying (8) with $\mathcal{A}_n = \mathcal{A}(S_n)$ and $\delta = n^{-1}$ gives, on the same event,

$$d_{\mu, \text{TV}}(\widehat{K}_n, K_0)^2 \leq \frac{C_{\text{fast}}}{(1-\varepsilon)^2 c_-} \left[\inf_{a \in \mathcal{A}_n} \mathcal{E}(a) + L_\ell n^{-1} + \delta_{\text{opt}} + \frac{\log\{2N_\infty^{\text{int}}(n^{-1}, \mathcal{A}_n)\} + \log(2/\eta)}{n} \right].$$

Using the same approximation and entropy estimates as above, we obtain

$$d_{\mu, \text{TV}}(\widehat{K}_n, K_0)^2 \leq C \left[n^{-2\beta/(2\beta+\bar{d})} (\log n)^\kappa + \delta_{\text{opt}} + \frac{\log(1/\eta)}{n} \right].$$

Combining the last two displays and recalling that $\bar{d} = 2d$, we obtain

$$\left\| \tilde{k}_n - k_0 \right\|_{2, \mu\lambda}^2 \vee d_{\mu, \text{TV}}(\widehat{K}_n, K_0)^2 \leq C \left[n^{-2\beta/(2\beta+2d)} (\log n)^\kappa + \delta_{\text{opt}} + \frac{\log(1/\eta)}{n} \right].$$

This proves the high-probability upper bound.

It remains to prove the minimax lower bound. It suffices to prove the lower bound on the submodel where $\mu = \lambda$ is Lebesgue probability measure on $[0, 1]^d$ and $r \equiv 1$, since a lower bound over a subclass is also a lower bound for the full class.

Choose nonzero functions $\varphi \in C_c^\infty((0, 1)^d)$ and $\psi \in C_c^\infty((0, 1)^d)$ such that

$$\int_{[0, 1]^d} \psi(y) dy = 0.$$

Set

$$b(x, y) := \varphi(x)\psi(y).$$

Then $b \in C_c^\infty((0, 1)^{2d})$, $b \not\equiv 0$, and

$$\int_{[0, 1]^d} b(x, y) dy = 0 \quad \text{for every } x.$$

For sufficiently small $h > 0$, choose $J_h \geq ch^{-2d}$ disjoint translates of the support of b inside $[0, 1]^{2d}$ and define

$$b_{j,h}(z) := h^\beta b\left(\frac{z - z_j}{h}\right), \quad z = (x, y), \quad j = 1, \dots, J_h.$$

The supports are disjoint, and

$$\int b_{j,h}(x, y) dy = 0 \quad \text{for every } x,$$

while

$$\|b_{j,h}\|_2^2 = h^{2\beta+2d} \|b\|_2^2.$$

The standard separated-bump scaling estimates imply that

$$\sum_{j=1}^{J_h} \theta_j b_{j,h}$$

has uniformly bounded \mathcal{H}_{2d}^β -norm over all $\theta \in \{0, 1\}^{J_h}$.

Choose $\omega > 0$ sufficiently small, depending only on (d, β, R, m, M) , so that for all sufficiently small h ,

$$k_\theta(x, y) := 1 + \omega \sum_{j=1}^{J_h} \theta_j b_{j,h}(x, y), \quad \theta \in \{0, 1\}^{J_h},$$

belongs to $\mathcal{K}_\beta(R, m, M)$. The zero-integral condition gives

$$\int_{[0,1]^d} k_\theta(y | x) dy = 1 \quad \text{for every } x,$$

and the smallness of ω ensures

$$m \leq k_\theta(y | x) \leq M.$$

Let P_θ be the one-sample law of (X, Y) under k_θ , and let P_θ^n be the law of n independent transition pairs. If $\theta^{(j)}$ differs from θ only in the j -th coordinate, then

$$k_\theta - k_{\theta^{(j)}} = \pm \omega b_{j,h}.$$

Since $k_{\theta^{(j)}} \geq m$,

$$\text{KL}(P_\theta \| P_{\theta^{(j)}}) \leq \int \frac{(k_\theta - k_{\theta^{(j)}})^2}{k_{\theta^{(j)}}} d\mu d\lambda \leq m^{-1} \omega^2 \|b_{j,h}\|_2^2.$$

By tensorization,

$$\text{KL}(P_\theta^n \| P_{\theta^{(j)}}^n) \leq nm^{-1} \omega^2 \|b\|_2^2 h^{2\beta+2d}.$$

Choose

$$h_n := c_h n^{-1/(2\beta+2d)}$$

with $c_h > 0$ sufficiently small so that the preceding KL divergence is bounded by a sufficiently small absolute constant. By Pinsker's inequality, neighboring experiments have total variation distance bounded away from one. Assouad's lemma then gives

$$\inf_{\hat{k}} \sup_{\theta \in \{0,1\}^{J_{h_n}}} \mathbb{E}_\theta \left\| \hat{k} - k_\theta \right\|_{2,\mu\lambda}^2 \geq c \omega^2 J_{h_n} h_n^{2\beta+2d}.$$

Since $J_{h_n} \geq c h_n^{-2d}$,

$$J_{h_n} h_n^{2\beta+2d} \geq c h_n^{2\beta}.$$

Therefore

$$\inf_{\hat{k}} \sup_{\theta \in \{0,1\}^{J_{h_n}}} \mathbb{E}_\theta \left\| \hat{k} - k_\theta \right\|_{2,\mu\lambda}^2 \geq c h_n^{2\beta} = c n^{-2\beta/(2\beta+2d)}.$$

Since the finite family $\{k_\theta : \theta \in \{0, 1\}^{J_{h_n}}\}$ is contained in $\mathcal{K}_\beta(R, m, M)$, it follows that

$$\inf_{\hat{k}} \sup_{K \in \mathcal{K}_\beta(R, m, M)} \mathbb{E}_K \left\| \hat{k} - k \right\|_{2,\mu\lambda}^2 \geq c n^{-2\beta/(2\beta+2d)}.$$

Finally, allowing the estimator to use independently generated reference variables does not improve the minimax risk: conditioning such an estimator on the observed transition pairs and applying Jensen's inequality gives an estimator based only on the transition pairs with no larger risk. Hence the same lower bound holds in the augmented experiment.

The upper and lower bounds together show that the squared $L^2(\mu \otimes \lambda)$ rate is minimax near-optimal up to logarithmic factors. The squared TV upper bound follows from the same estimator through Theorem 9, and no separate TV minimax lower bound is claimed.

A.7 Proof of Theorem 12

This subsection proves the finite-horizon dynamic transfer result used in Section 6. The proof is a standard occupancy-weighted perturbation argument, followed by the calibration and Markovization bounds from the main text.

Before presenting the complete proof of Theorem 12, we first introduce the following lemma.

Lemma 21 (Occupancy-weighted finite-horizon perturbation) *Let K and L be Markov kernels, let ξ be an initial law, and set*

$$e_{K,L}(x) := \text{TV}(K(x, \cdot), L(x, \cdot)).$$

For every integer $m \geq 1$,

$$\text{TV}(\xi K^m, \xi L^m) \leq \sum_{s=0}^{m-1} \int e_{K,L}(x) (\xi K^s)(dx).$$

The same right-hand side also bounds the total variation distance between the length- m path laws generated from the common initial law ξ and kernels K and L .

Proof For the marginal law, write

$$\text{TV}(\xi K^m, \xi L^m) \leq \text{TV}(\xi K^m, \xi K^{m-1}L) + \text{TV}(\xi K^{m-1}L, \xi L^m).$$

The first term is bounded by

$$\int e_{K,L}(x) (\xi K^{m-1})(dx),$$

and the second is at most $\text{TV}(\xi K^{m-1}, \xi L^{m-1})$ by TV contraction under Markov kernels. Iterating this recursion from m down to 1 gives the displayed bound.

For path laws, let $P_K^{(m)}$ and $P_L^{(m)}$ denote the laws of (X_0, \dots, X_m) generated from ξ under K and L . Let Q_j be the path law using K for the first j transitions and L for the remaining $m-j$ transitions, so that $Q_0 = P_L^{(m)}$ and $Q_m = P_K^{(m)}$. The neighboring laws Q_j and Q_{j+1} agree up to time j , where the state has law ξK^j . Replacing the next conditional kernel from L to K changes the joint law by at most

$$\int e_{K,L}(x) (\xi K^j)(dx),$$

and appending the same remaining L -transitions is a TV contraction. Summing over $j = 0, \dots, m-1$ proves the path-law bound. \blacksquare

We now present the complete proof of Theorem 12.

Part (i). Apply Lemma 21 with $K = K_0$ and $L = \widehat{K}$. For

$$e(x) := \text{TV}(K_0(x, \cdot), \widehat{K}(x, \cdot)),$$

we obtain

$$\text{TV}(\xi K_0^m, \xi \widehat{K}^m) \leq \sum_{s=0}^{m-1} \int e(x) (\xi K_0^s)(dx).$$

If $f_s = d(\xi K_0^s)/d\mu$ and $C_s = \text{ess sup}_\mu f_s$, then

$$\int e(x) (\xi K_0^s)(dx) = \int e(x) f_s(x) \mu(dx) \leq C_s \int e(x) \mu(dx).$$

Since $\int e d\mu = d_{\mu, \text{TV}}(K_0, \widehat{K})$, summing over $s = 0, \dots, m-1$ gives the L^1 -coverage bound

$$\text{TV}(\xi K_0^m, \xi \widehat{K}^m) \leq \left(\sum_{s=0}^{m-1} C_s \right) d_{\mu, \text{TV}}(K_0, \widehat{K}).$$

Part (ii). For the L^2 version, $0 \leq f_s \leq C_s$ and $\int f_s d\mu = 1$ imply

$$\|f_s\|_{L^2(\mu)}^2 \leq C_s.$$

Thus Cauchy–Schwarz gives

$$\int e(x) (\xi K_0^s)(dx) \leq \sqrt{C_s} \|e\|_{L^2(\mu)} \leq \sqrt{C_{\xi, \mu, m}} \|e\|_{L^2(\mu)},$$

where $C_{\xi, \mu, m} := \max_{0 \leq s < m} C_s$. Summing over s yields

$$\text{TV}(\xi K_0^m, \xi \widehat{K}^m) \leq m \sqrt{C_{\xi, \mu, m}} \|e\|_{L^2(\mu)}.$$

The same argument applied to the path-law part of Lemma 21 gives the identical bound for length- m path laws.

Part (iii). For normalized occupation measures,

$$\bar{\Gamma}_m^K := \frac{1}{m} \sum_{t=0}^{m-1} \xi K^t,$$

the triangle inequality and the preceding marginal bound give

$$\begin{aligned} \text{TV}(\bar{\Gamma}_m^{K_0}, \bar{\Gamma}_m^{\widehat{K}}) &\leq \frac{1}{m} \sum_{t=0}^{m-1} \text{TV}(\xi K_0^t, \xi \widehat{K}^t) \\ &\leq \frac{1}{m} \sum_{t=0}^{m-1} t \sqrt{C_{\xi, \mu, m}} \|e\|_{L^2(\mu)} \\ &= \frac{m-1}{2} \sqrt{C_{\xi, \mu, m}} \|e\|_{L^2(\mu)}. \end{aligned}$$

It remains to connect $\|e\|_{L^2(\mu)}$ to contrastive excess risk. Let

$$\tilde{k}_{\hat{a}} := \frac{\hat{a} - \varepsilon r}{1 - \varepsilon}, \quad \hat{k} := \mathfrak{M}\tilde{k}_{\hat{a}}.$$

By Theorem 9, applied pointwise in x with $g = \tilde{k}_{\hat{a}}$ and $k = k_0$,

$$e(x) = \frac{1}{2} \int |\hat{k}(y | x) - k_0(y | x)| \lambda(dy) \leq \int |\tilde{k}_{\hat{a}}(y | x) - k_0(y | x)| \lambda(dy).$$

Because λ is a probability measure, Cauchy–Schwarz in y gives

$$e(x)^2 \leq \int |\tilde{k}_{\hat{a}}(y | x) - k_0(y | x)|^2 \lambda(dy).$$

After integrating in x ,

$$\|e\|_{L^2(\mu)} \leq \|\tilde{k}_{\hat{a}} - k_0\|_{L^2(\mu \otimes \lambda)}.$$

The calibration theorem gives

$$\|\tilde{k}_{\hat{a}} - k_0\|_{L^2(\mu \otimes \lambda)}^2 \leq \frac{1}{(1 - \varepsilon)^2 c_-} \mathcal{E}(\hat{a}).$$

Combining the last two displays with the L^2 -coverage bounds proves

$$\text{TV}(\xi K_0^m, \xi \hat{K}^m) \leq \frac{m \sqrt{C_{\xi, \mu, m}}}{(1 - \varepsilon) \sqrt{c_-}} \mathcal{E}(\hat{a})^{1/2},$$

and the corresponding normalized-occupation bound with m replaced by $(m - 1)/2$.

Corollary 22 (Invariant law perturbation under contraction) *Let K and L have invariant laws π_K and π_L . If*

$$\alpha(K) := \sup_{x, x'} \text{TV}(K(x, \cdot), K(x', \cdot)) < 1,$$

then

$$\text{TV}(\pi_K, \pi_L) \leq \frac{d_{\infty, \text{TV}}(K, L)}{1 - \alpha(K)}, \quad d_{\infty, \text{TV}}(K, L) := \sup_x \text{TV}(K(x, \cdot), L(x, \cdot)).$$

Proof By invariance of π_K and π_L ,

$$\pi_K = \pi_K K, \quad \pi_L = \pi_L L.$$

Therefore, by the triangle inequality,

$$\begin{aligned} \text{TV}(\pi_K, \pi_L) &= \text{TV}(\pi_K K, \pi_L L) \\ &\leq \text{TV}(\pi_K K, \pi_L K) + \text{TV}(\pi_L K, \pi_L L). \end{aligned}$$

The first term is controlled by the Dobrushin contraction coefficient:

$$\text{TV}(\pi_K K, \pi_L K) \leq \alpha(K) \text{TV}(\pi_K, \pi_L).$$

For the second term, use convexity of total variation under mixtures:

$$\begin{aligned} \text{TV}(\pi_L K, \pi_L L) &= \text{TV} \left(\int K(x, \cdot) \pi_L(\mathrm{d}x), \int L(x, \cdot) \pi_L(\mathrm{d}x) \right) \\ &\leq \int \text{TV}(K(x, \cdot), L(x, \cdot)) \pi_L(\mathrm{d}x) \\ &\leq d_{\infty, \text{TV}}(K, L). \end{aligned}$$

Combining the two bounds gives

$$\text{TV}(\pi_K, \pi_L) \leq \alpha(K) \text{TV}(\pi_K, \pi_L) + d_{\infty, \text{TV}}(K, L).$$

Since $\alpha(K) < 1$, moving the first term to the left-hand side yields

$$(1 - \alpha(K)) \text{TV}(\pi_K, \pi_L) \leq d_{\infty, \text{TV}}(K, L).$$

Dividing by $1 - \alpha(K)$ proves the claim. ■

A.8 Proof of Theorem 14

For two sigma-fields \mathcal{G} and \mathcal{H} , define

$$\beta(\mathcal{G}, \mathcal{H}) := \frac{1}{2} \sup \sum_{i,j} |\mathbb{P}(G_i \cap H_j) - \mathbb{P}(G_i)\mathbb{P}(H_j)|,$$

where the supremum is over all pairs of finite measurable partitions $(G_i)_i$ and $(H_j)_j$ of the underlying sample space, with $G_i \in \mathcal{G}$ and $H_j \in \mathcal{H}$. With this normalization, Berbee's coupling lemma gives a mismatch probability bounded by the corresponding absolute-regularity coefficient.

Write $M = \lfloor N/q \rfloor$ and define the retained augmented blocks

$$B_j^{(q)} := (X_{jq-1}, X_{jq}, \tilde{Y}_j, Z_{j1}, \dots, Z_{j\tau}), \quad j = 1, \dots, M.$$

The auxiliary variables are independent across retained transitions and independent of the trajectory. Appending such variables does not increase the absolute-regularity coefficient of the retained sequence. The j th retained transition ends at time jq , while the next retained transition begins at time $(j+1)q - 1$, so consecutive retained blocks are separated by $(j+1)q - 1 - jq = q - 1$ time steps.

By Berbee's coupling lemma for absolutely regular sequences (Berbee, 1979; Doukhan, 1994), there exist independent blocks B_1^*, \dots, B_M^* , each B_j^* having the same marginal law as $B_j^{(q)}$, such that

$$\mathbb{P} \left[(B_1^{(q)}, \dots, B_M^{(q)}) \neq (B_1^*, \dots, B_M^*) \right] \leq (M-1)\beta_X(q-1).$$

The assumed thinning condition gives

$$(M-1)\beta_X(q-1) \leq \eta/2.$$

By stationarity,

$$(X_{jq-1}, X_{jq}) \sim \mu(dx)K_0(x, dy),$$

and the auxiliary variables have exactly the same conditional distribution as in the independent blocks used in Theorem 7. Hence B_1^*, \dots, B_M^* are i.i.d. copies of that block distribution.

On the coupling event, the thinned trajectory empirical risk and the coupled independent empirical risk coincide pointwise over \mathcal{A}_M . Hence $\widehat{a}_{M,q}^{\text{tr}}$, which is a measurable δ_{opt} -approximate minimizer of the thinned trajectory risk, is also a δ_{opt} -approximate minimizer of the coupled independent empirical risk on that event. The proof of Theorem 7(iii) constructs a concentration event, depending only on the independent sample blocks, on which the deterministic oracle argument applies simultaneously to every measurable δ_{opt} -approximate empirical-risk minimizer over \mathcal{A}_M . Apply this uniform concentration event to the coupled independent blocks with sample size M , candidate class \mathcal{A}_M , and confidence level $\eta/2$. A union bound with the coupling failure event yields, with probability at least $1 - \eta$,

$$\mathcal{E}(\widehat{a}_{M,q}^{\text{tr}}) \leq C_{\text{or}} \mathfrak{R}_{M,q}(\eta, \delta),$$

after absorbing the numerical factor $5/3$ and the constant C_{fast} from Theorem 7(iii) into C_{or} .

The calibration consequence gives

$$\left\| \widetilde{k}_{M,q}^{\text{tr}} - k_0 \right\|_{2,\mu\lambda}^2 \leq \frac{1}{(1-\varepsilon)^2 c_-} \mathcal{E}(\widehat{a}_{M,q}^{\text{tr}}) \leq C \mathfrak{R}_{M,q}(\eta, \delta).$$

By the definition of integrated total variation, Theorem 9, and Cauchy–Schwarz under the probability measure $\mu \otimes \lambda$,

$$\begin{aligned} d_{\mu, \text{TV}}(\widehat{K}_{M,q}^{\text{tr}}, K_0) &= \frac{1}{2} \left\| \mathfrak{M} \widetilde{k}_{M,q}^{\text{tr}} - k_0 \right\|_{1,\mu\lambda} \\ &\leq \left\| \widetilde{k}_{M,q}^{\text{tr}} - k_0 \right\|_{1,\mu\lambda} \\ &\leq \left\| \widetilde{k}_{M,q}^{\text{tr}} - k_0 \right\|_{2,\mu\lambda}. \end{aligned}$$

Squaring gives

$$d_{\mu, \text{TV}}(\widehat{K}_{M,q}^{\text{tr}}, K_0)^2 \leq C_{\text{ker}} \mathfrak{R}_{M,q}(\eta, \delta).$$

The marginal, path-law, and normalized occupation-measure bounds then follow from Theorem 12, with constants absorbed into C_{dyn} .

A.9 Proof of Corollary 15

By the definition of $q_{N,\eta}$, we have $q_{N,\eta} \geq 2$ and

$$B\rho^{q_{N,\eta}-1} \leq \frac{\eta}{2N}.$$

Since $M = N_{\text{eff}} \leq N$, it follows that

$$(M-1)\beta_X(q_{N,\eta}-1) \leq NB\rho^{q_{N,\eta}-1} \leq \eta/2.$$

Thus the thinning condition in Theorem 14 holds with $q = q_{N,\eta}$ and $M = N_{\text{eff}}$, and all conclusions of that theorem apply. The displayed order of N_{eff} follows directly from $q_{N,\eta} = O(\log(N/\eta))$.

A.10 Proof of Proposition 17

Let

$$K_\rho = \begin{pmatrix} 1/2 & 1/2 \\ 1/2 & 1/2 \end{pmatrix}, \quad L_\rho = \begin{pmatrix} 1/2 & 1/2 \\ 1/10 & 9/10 \end{pmatrix}.$$

Both kernels are irreducible. Their first rows agree, while the total variation distance between their second rows is $2/5$. Put

$$s_\rho := \min\{(5/2)\rho, 1\}, \quad \mu_\rho = (1 - s_\rho)\delta_0 + s_\rho\delta_1.$$

Then

$$d_{\mu_\rho, \text{TV}}(K_\rho, L_\rho) = \frac{2}{5}s_\rho \leq \rho.$$

The invariant law of K_ρ is $(1/2, 1/2)$. Solving $\pi_{L_\rho} = \pi_{L_\rho} L_\rho$ gives

$$\pi_{L_\rho}(1) = \frac{1/2}{1/2 + 1/10} = \frac{5}{6}.$$

Therefore

$$\text{TV}(\pi_{K_\rho}, \pi_{L_\rho}) = |\pi_{L_\rho}(1) - 1/2| = \frac{1}{3} \geq \frac{1}{4}.$$

References

- Yacine Aït-Sahalia. Maximum likelihood estimation of discretely sampled diffusions: A closed-form approximation approach. *Econometrica*, 70(1):223–262, 2002. doi: 10.1111/1468-0262.00274.
- Martin Anthony and Peter L. Bartlett. *Neural Network Learning: Theoretical Foundations*. Cambridge University Press, Cambridge, 1999. doi: 10.1017/CBO9780511624216.
- Peter L Bartlett and Shahar Mendelson. Rademacher and gaussian complexities: Risk bounds and structural results. *Journal of machine learning research*, 3(Nov):463–482, 2002.
- Peter L. Bartlett, Olivier Bousquet, and Shahar Mendelson. Local Rademacher complexities. *The Annals of Statistics*, 33(4):1497–1537, 2005. doi: 10.1214/009053605000000282.
- Peter L. Bartlett, Nick Harvey, Christopher Liaw, and Abbas Mehrabian. Nearly-tight VC-dimension and pseudodimension bounds for piecewise linear neural networks. *Journal of Machine Learning Research*, 20(63):1–17, 2019. URL <https://www.jmlr.org/papers/v20/17-612.html>.
- H. C. P. Berbee. *Random Walks with Stationary Increments and Renewal Theory*, volume 112 of *Mathematical Centre Tracts*. Mathematisch Centrum, Amsterdam, 1979.

- Christopher M. Bishop. Mixture density networks. Neural Computing Research Group Report NCRG/94/004, Aston University, 1994.
- Stéphane Boucheron, Gábor Lugosi, and Pascal Massart. *Concentration Inequalities: A Nonasymptotic Theory of Independence*. Oxford University Press, Oxford, 2013. doi: 10.1093/acprof:oso/9780199535255.001.0001.
- Ciwan Ceylan and Michael U. Gutmann. Conditional noise-contrastive estimation of unnormalised models. In *Proceedings of the 35th International Conference on Machine Learning*, volume 80 of *Proceedings of Machine Learning Research*, pages 726–734. PMLR, 2018. URL <https://proceedings.mlr.press/v80/ceylan18a.html>.
- Xiaohong Chen. Large sample sieve estimation of semi-nonparametric models. In James J. Heckman and Edward E. Leamer, editors, *Handbook of Econometrics*, volume 6B, chapter 76, pages 5549–5632. Elsevier, 2007. doi: 10.1016/S1573-4412(07)06076-X.
- Xiaohong Chen and Xiaotong Shen. Sieve extremum estimates for weakly dependent data. *Econometrica*, 66(2):289–314, 1998. doi: 10.2307/2998559.
- Kurtland Chua, Roberto Calandra, Rowan McAllister, and Sergey Levine. Deep reinforcement learning in a handful of trials using probabilistic dynamics models. In *Advances in neural information processing systems*, volume 31, 2018.
- Roland L Dobrushin. Central limit theorem for nonstationary markov chains. i. *Theory of Probability & Its Applications*, 1(1):65–80, 1956.
- Paul Doukhan. *Mixing: Properties and Examples*, volume 85 of *Lecture Notes in Statistics*. Springer, New York, 1994. doi: 10.1007/978-1-4612-2642-0.
- Zijun Gao and Trevor Hastie. LinCDE: Conditional density estimation via Lindsey’s method. *Journal of Machine Learning Research*, 23(52):1–55, 2022. URL <https://www.jmlr.org/papers/v23/21-0840.html>.
- Michael U. Gutmann and Aapo Hyvärinen. Noise-contrastive estimation of unnormalized statistical models, with applications to natural image statistics. *Journal of Machine Learning Research*, 13(11):307–361, 2012. URL <https://www.jmlr.org/papers/v13/gutmann12a.html>.
- David Ha and Jürgen Schmidhuber. World models. *arXiv preprint arXiv:1803.10122*, 2018. doi: 10.48550/arXiv.1803.10122.
- Danijar Hafner, Timothy Lillicrap, Jimmy Ba, and Mohammad Norouzi. Dream to control: Learning behaviors by latent imagination. In *Proceedings of the International Conference on Learning Representations*, 2020. URL <https://openreview.net/forum?id=S110TC4tDS>.
- Peter Hall and Qiwei Yao. Approximating conditional distribution functions using dimension reduction. *The Annals of Statistics*, 33(3):1404–1421, 2005. doi: 10.1214/009053604000001282.

- Peter Hall, Rodney C. L. Wolff, and Qiwei Yao. Methods for estimating a conditional distribution function. *Journal of the American Statistical Association*, 94(445):154–163, 1999. doi: 10.1080/01621459.1999.10473832.
- Peter Hall, Jeffrey S. Racine, and Qi Li. Cross-validation and the estimation of conditional probability densities. *Journal of the American Statistical Association*, 99(468):1015–1026, 2004. doi: 10.1198/016214504000000548.
- Lars Peter Hansen, José A. Scheinkman, and Nizar Touzi. Spectral methods for identifying scalar diffusions. *Journal of Econometrics*, 86(1):1–32, 1998. doi: 10.1016/S0304-4076(97)00107-3.
- Rob J. Hyndman and Qiwei Yao. Nonparametric estimation and symmetry tests for conditional density functions. *Journal of Nonparametric Statistics*, 14(3):259–278, 2002. doi: 10.1080/10485250212374.
- Rafael Izbicki and Ann B. Lee. Converting high-dimensional regression to high-dimensional conditional density estimation. *Electronic Journal of Statistics*, 11, 2017.
- Michael Janner, Justin Fu, Marvin Zhang, and Sergey Levine. When to trust your model: Model-based policy optimization. In *Advances in Neural Information Processing Systems*, volume 32, pages 12498–12509, 2019. URL https://papers.nips.cc/paper_files/paper/2019/hash/5faf461eff3099671ad63c6f3f094f7f-Abstract.html.
- Mykola V. Kartashov. *Strong Stable Markov Chains*. VSP, Utrecht, 1996.
- Vladimir Koltchinskii. Local Rademacher complexities and oracle inequalities in risk minimization. *The Annals of Statistics*, 34(6):2593–2656, 2006. doi: 10.1214/009053606000001019.
- Guillaume Lecué and Charles Mitchell. Oracle inequalities for cross-validation type procedures. *Electronic Journal of Statistics*, 6:1803–1837, 2012.
- Chenghao Li and Yuanyuan Lin. A data-augmented contrastive learning approach to non-parametric density estimation. *Journal of Machine Learning Research*, 27(10):1–47, 2026. URL <https://www.jmlr.org/papers/v27/25-0376.html>.
- Michael Li, Matey Neykov, and Sivaraman Balakrishnan. Minimax optimal conditional density estimation under total variation smoothness. *Electronic Journal of Statistics*, 16(2):3937–3972, 2022.
- Sean P. Meyn and Richard L. Tweedie. *Markov Chains and Stochastic Stability*. Cambridge University Press, Cambridge, 2 edition, 2009.
- A. Yu. Mitrophanov. Sensitivity and convergence of uniformly ergodic markov chains. *Journal of Applied Probability*, 42(4):1003–1014, 2005. doi: 10.1239/jap/1134587812.
- Eero Nummelin. A splitting technique for Harris recurrent Markov chains. *Zeitschrift für Wahrscheinlichkeitstheorie und Verwandte Gebiete*, 43(4):309–318, 1978. doi: 10.1007/BF00534764.

- Johannes Schmidt-Hieber. Nonparametric regression using deep neural networks with ReLU activation function. *The Annals of Statistics*, 48(4):1875–1897, 2020. doi: 10.1214/19-AOS1875.
- Charles J. Stone. Optimal global rates of convergence for nonparametric regression. *The Annals of Statistics*, 10(4):1040–1053, 1982. doi: 10.1214/aos/1176345969.
- Masashi Sugiyama, Taiji Suzuki, and Takafumi Kanamori. *Density Ratio Estimation in Machine Learning*. Cambridge University Press, Cambridge, 2012. doi: 10.1017/CBO9781139035613.
- Erik Talvitie. Model regularization for stable sample rollouts. In *UAI*, pages 780–789, 2014.
- Brian L. Trippe and Richard E. Turner. Conditional density estimation with bayesian normalising flows. *arXiv preprint arXiv:1802.04908*, 2018. doi: 10.48550/arXiv.1802.04908.
- Alexandre B. Tsybakov. Optimal aggregation of classifiers in statistical learning. *The Annals of Statistics*, 32(1):135–166, 2004. doi: 10.1214/aos/1079120131.
- Roman Vershynin. *High-Dimensional Probability: An Introduction with Applications in Data Science*. Cambridge University Press, Cambridge, 2018. doi: 10.1017/9781108231596.
- Martin J Wainwright. *High-dimensional statistics: A non-asymptotic viewpoint*, volume 48. Cambridge university press, 2019.
- Dmitry Yarotsky. Error bounds for approximations with deep ReLU networks. *Neural Networks*, 94:103–114, 2017. doi: 10.1016/j.neunet.2017.07.002.